



ELSEVIER

Available online at www.sciencedirect.com

SCIENCE @ DIRECT®

Journal of African Earth Sciences xxx (2005) xxx–xxx

Journal of African
Earth Sciences

www.elsevier.com/locate/jafrearsci

Metamorphic evolution of the Maud Belt: P – T – t path for high-grade gneisses in Gjelsvikfjella, Dronning Maud Land, East Antarctica

Avinash Bisnath^{*}, Hartwig E. Frimmel¹*Department of Geological Sciences, University of Cape Town, Private Bag, Rondebosch 7701, Cape Town, South Africa*

Received 11 March 2005; received in revised form 8 August 2005; accepted 11 September 2005

Abstract

A metamorphic petrological study, in conjunction with recent precise geochronometric data, revealed a complex P – T – t path for high-grade gneisses in a hitherto poorly understood sector of the Mesoproterozoic Maud Belt in East Antarctica. The Maud Belt is an extensive high-grade, polydeformed, metamorphic belt, which records two significant tectono-thermal episodes, once towards the end of the Mesoproterozoic and again towards the late Neoproterozoic/Cambrian. In contrast to previous models, most of the metamorphic mineral assemblages are related to a Pan-African tectono-thermal overprint, with only very few relics of late Mesoproterozoic granulite-facies mineral assemblages (M_1) left in strain-protected domains. Petrological and mineral chemical evidence indicates a clockwise P – T – t path for the Pan-African orogeny. Peak metamorphic (M_{2b}) conditions recorded by most rocks in the area ($T = 709$ – 785 °C and $P = 7.0$ – 9.5 kbar) during the Pan-African orogeny were attained subsequent to decompression from probably eclogite-facies metamorphic conditions (M_{2a}).

The new data acquired in this study, together with recent geochronological and geochemical data, permit the development of a geodynamic model for the Maud Belt that involves volcanic arc formation during the late Mesoproterozoic followed by extension at 1100 Ma and subsequent high-grade tectono-thermal reworking once during continent–continent collision at the end of the Mesoproterozoic (M_1 ; 1090–1030 Ma) and again during the Pan-African orogeny (M_{2a} , M_{2b}) between 565 and 530 Ma. Post-peak metamorphic K-metasomatism under amphibolite-facies conditions (M_{2c}) followed and is ascribed to post-orogenic bimodal magmatism between 500 and 480 Ma.

© 2005 Published by Elsevier Ltd.

Keywords: Maud belt; Gjelsvikfjella; Pan-African orogeny; P – T – t path; East Antarctica

1. Introduction

Dronning Maud Land in East Antarctica contains useful information for the understanding of both the amalgamation and fragmentation of supercontinents, once towards the end of the Mesoproterozoic at ca. 1.2–1.0 Ga (equivalent to the ‘Grenvillian’ of North America) and again at the end of the Neoproterozoic/early Palaeozoic

at ca. 0.6–0.5 Ga (the ‘Pan-African’ of Africa). The tectonic framework of East Antarctica is dominated by the East Antarctic Craton (Tingey, 1991; Krynauw, 1996), comprising fragments of Archaean continental crust (e.g. the Grunehogna Craton) surrounded by younger orogenic belts, such as the Maud Belt (traditionally referred to as the Maudheim Province; Fig. 1). Rocks of the Maud Belt are exposed, from southwest to northeast, in the Heimefrontfjella, the Kirwanveggen, the H.U. Sverdrupfjella, the Gjelsvikfjella and western Mühlig-Hofmannfjella (Fig. 1). The belt is dominated by Mesoproterozoic supracrustal and intrusive rocks that were intruded by Neoproterozoic and early Palaeozoic granitoids (Arndt et al., 1991; Moyes and Groenewald, 1996; Jackson, 1999; Jacobs et al., 1999;

^{*} Corresponding author. Current address: Council for Geoscience, P.O. Box 900, Pietermaritzburg 3200, South Africa. Tel.: +27 33 345 6265/27 84 560 5006; fax: +27 33 394 9342.

E-mail address: abisnath@geology.uct.ac.za (A. Bisnath).

¹ Current address: Institute of Mineralogy, University of Würzburg, Am Hubland, D-97074 Würzburg, Germany.

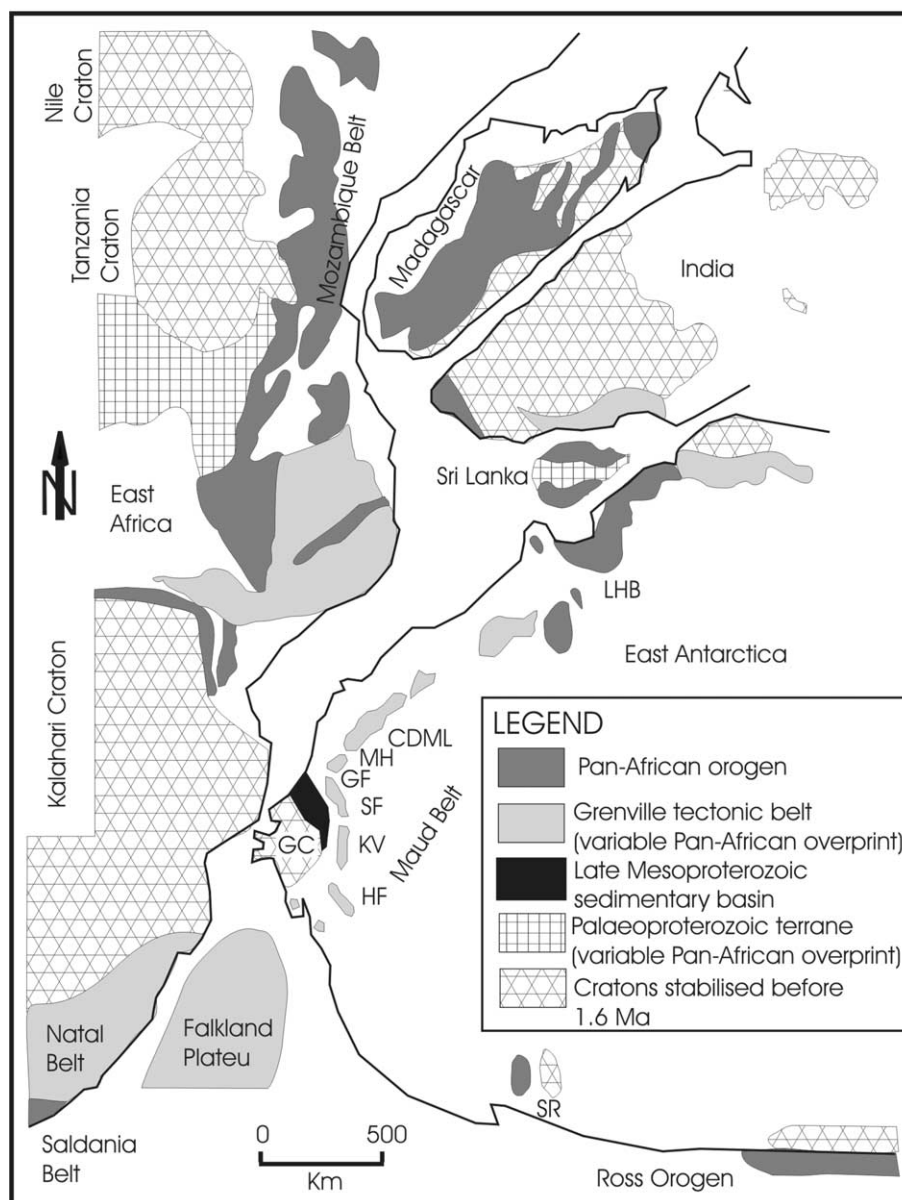


Fig. 1. Map showing correlations between Africa and East Antarctica within a Gondwana framework (from Frimmel, 2004). Abbreviations are: Heimefrontfjella (HF), Kirwanveggen (KV), H.U. Sverdrupfjella (SF), Gjelsvikfjella (GF), Mühlig-Hofmannfjella (MH), Central Dronning Maud Land (CDML), Lützow-Holm Bay (LHB), Shackleton Range (SR) and Grunehogna Province (GP).

48 Paulsson and Austrheim, 2003). In late Precambrian palaeo-
 49 ogeographic reconstructions, the Maud Belt is typically
 50 placed as part of the Kalahari Craton (e.g. Hoffman,
 51 1991; Dalziel, 1997), which amalgamated with East Antarc-
 52 tica to form Gondwana between 570 and 530 Ma (Meert
 53 and Van der Voo, 1997; Meert, 2003).

54 In the past, the penetrative foliation in the Maud Belt
 55 has been suggested to be Mesoproterozoic in age (Groene-
 56 wald et al., 1995; Grantham et al., 1995; Jackson, 1999)
 57 implying that the Maud Belt was a continuous tectonic belt
 58 not only from Heimefrontfjella to central Dronning Maud
 59 Land but also beyond East Antarctica, linking up with the
 60 Namaqua–Natal Belt in South Africa. More recent geo-
 61 chronological data (Jacobs et al., 1998; Bisnath et al.,

2004; Board et al., in press), however, point to major struc-
 62 tural reworking of the Mesoproterozoic crust in the belt
 63 during the Pan-African orogeny.

64
 65 A strong Pan-African thermal overprint and melt gener-
 66 ation has been documented for central Dronning Maud
 67 Land (Jacobs et al., 1998), where a Pan-African age has
 68 been suggested for pervasive east–west trending structures
 69 (Jacobs et al., 2003a,b,d). Similarly, a Pan-African age
 70 (530–540 Ma) has been suggested for the penetrative folia-
 71 tion in the H.U. Sverdrupfjella, where it follows a north-
 72 east–southwest trend (Board et al., in press). This study
 73 focuses on the poorly documented outcrops of Gjelsvikfj-
 74 ella (between 2° to 5°35'E and 71°46' to 72°15'S), which
 75 is located in between the above two areas, and where the

76 two different principal structural trends seemingly intersect
77 (Fig. 1).

78 In this contribution, the tectono-thermal regimes at
79 which the respective Mesoproterozoic and Neoproterozoic
80 deformation took place in the Gjelsvikfjella area are
81 assessed. In order to resolve the complex thermal history
82 of the area, detailed petrography and geothermobaromet-
83 ric studies were carried out to generate, in conjunction with
84 new geochronological data (Bisnath et al., 2004) a coherent
85 pressure–temperature–time (P – T – t) path and to establish a
86 geodynamic model for this part of the Maud Belt.

87 2. Regional geology of the Maud Belt

88 The Maud Belt consists of late Mesoproterozoic to early
89 Cambrian polyphase deformed upper amphibolite- to
90 granulite-facies metamorphic rocks and a variety of post-
91 tectonic intrusions (Table 1). The belt is separated by large
92 glaciers (Jutulstraumen–Pencksökket glacier) from the
93 Grunehogna Craton to the northwest, which consists of
94 Archaean granite overlain by the Mesoproterozoic vol-
95 cano-sedimentary Ritscherflya Supergroup (Wolmarans
96 and Kent, 1982; Moyes et al., 1995). The oldest rocks rec-
97 ognized in the Maud Belt are paragneisses and felsic- to
98 intermediate-metavolcanic rocks that yielded U–Pb zircon
99 ages of between 1160 and 1140 Ma (Arndt et al., 1991;
100 Harris et al., 1995; Jacobs et al., 1998; Paulsson and Aus-
101 trheim, 2003; Board et al., in press). The oldest intrusive
102 rocks (meta-tonalitic gneisses) in the Maud Belt (from wes-
103 tern to central Dronning Maud Land; Fig. 1) preserve sim-
104 ilar ages of between 1140 and 1130 Ma (Table 2; Jackson,
105 1999; Jacobs et al., 1998; Paulsson and Austrheim, 2003;
106 Bisnath et al., 2004; Board et al., in press). The overall
107 calc-alkaline signature of these rocks is consistent with
108 the interpretation of them forming part of a large volcanic

arc system (Groenewald et al., 1995; Jacobs et al., 1998; 109
Bauer et al., 2003), with highly variable, in places Archaean 110
Nd model ages pointing to derivation from an old, hetero- 111
geneous, sublithospheric mantle (E. Grosch and A. Bis- 112
nath, unpublished data, 2004). 113

The Ritscherflya Supergroup contains detritus that was 114
fed from an active volcanic arc system (Basson et al., 2004). 115
Magmatic zircon ages of 1131 ± 7 Ma from pyroclastic 116
beds in the lower Ritscherflya Supergroup (Frimmel, 117
2004) indicate sediment deposition contemporaneously 118
with volcanic arc formation. Consequently, the deposi- 119
tional centre for the Ritscherflya Supergroup is assumed 120
to have been adjacent to the Maud volcanic arc. 121

Megacrystic orthogneiss occurs throughout the Maud 122
Belt. Examples are the Fugitive, Isingen and Sveabreen 123
megacrystic orthogneiss of H.U. Sverdrupfjella (Groene- 124
wald et al., 1995), and the megacrystic orthogneiss bodies 125
of the Kirwanveggen (Grantham et al., 1995; Harris, 126
1999). Locally the alkali feldspar megacrysts display 127
resorption rims suggesting that they are older than the 128
matrix (Frimmel, 2004). This is supported by two distinct 129
SHRIMP U–Pb zircon ages of 1127 ± 12 and 130
 1061 ± 14 Ma obtained on megacrystic orthogneiss from 131
northern Kirwanveggen, which have been interpreted as 132
the age of crystallization and metamorphic matrix recryst- 133
tallization, respectively (Harris et al., 1995). 134

U–Pb single zircon ages of approximately 1128 ± 19 and 135
 1104 ± 8 Ma have been obtained for augen gneiss and 136
mylonitic augen gneiss units in the Gjelsvikfjella area (Bis- 137
nath et al., 2004). The older age group around 1128 Ma 138
conforms to the final stages of arc development and the 139
megacrystic granitic protoliths are therefore interpreted 140
as products of arc magmatism. 141

SHRIMP U–Pb zircon ages of between 1090 and 142
1030 Ma that are interpreted to record Grenvillian meta- 143

Table 1
Summary of the tectono-thermal evolution of the Maud Belt

	Eastern Heimefrontfjella (Jacobs et al., 1996)	Kirwanveggen (Grantham et al., 1995)	H.U. Sverdrupfjella (Grantham et al., 1995; Board et al., in press)	Gjelsvikfjella and Muhlig-Hofmannfjella (Bauer and Jacobs, 2001; Paulsson and Austrheim, 2003; Bisnath et al., 2004)
	<i>Volcanic island arc magmatism: 1120–1150 Ma</i>			
Lithology	Bimodal metavolcanic sequence, with pre- and syn-tectonic calc-alkaline granitoids	Migmatitic banded gneisses, minor biotite–garnet gneisses, interlayered with amphibolites and syntectonic mega-crystic orthogneisses	Quartzo-feldspathic and pelitic gneisses, various metamafic, marble and megacrystic orthogneisses	Migmatitic tonalitic quartzo- feldspathic, para- and orthogneisses, metasediments and megacrystic augen gneisses
D1?	Instruction of tabular megacrystic orthogneisses units; Magmatism related to Grenvillian orogeny? Metamorphism (M1?) and Deformation (D1?): 1100–1080 Ma			
D1?	High pressure eclogite facies metamorphism (D1?) and metamorphism (M1/M2a?): ca. 570 Ma			
D2	Main penetrative deformation episode and metamorphism (M2b): ca. 530 Ma			
D3	Pan-African intrusions and biotitization (M2c) ca. 510 Ma			
	Post-tectonic aplite intrusions: 500–480 Ma			
D4	Regional warping and folding: NE–SW trends			
D5	Gondwana breakup and dolerite dyke intrusions: 170 Ma			

e.g. Stabben meta-gabbro ca. 490 Ma

Table 2
Summary of the most reliable age data (all ages in Ma) for the Maud Belt, Antarctica

Rock type/mineral dated	Central Kirwangeggen Southwest (Jackson, 1999)	Northern Kirwanveggen (Harris et al., 1995)	Sverdrupfjella (Board et al., in press)	Gjelsvjkfjella (Bisnath et al., 2004)	Festninga/Risemedet (Jacobs et al., 2003a,b,d)	Central Dronning Maud Land Northeast (Jacobs et al., 1998, 2003c)
Stabben Gabbro				483 ± 11 487.3 ± 4.4		
Granite/Aplite Dykes		475 ± 10	480 ± 13	497 ± 5	486.9 ± 3.8	
Stabben Syenite				500 ± 8		
Zircon Overgrowths (Rims)				504 ± 6		
Lamprophyre Dyke					523 ± 4.8	
Chamokite					521.3 ± 3.4	
Zwiesel Gabbro						527 ± 5
Zircon Overgrowths (Rims)			528 ± 6	529 ± 4	528 ± 10	ca. 530
Syn-tectonic monazite			539 ± 9			
Granite Leucosome					558 ± 5.6	
Zircon Overgrowths (Rims)		585 ± 20	565 ± 11	ca. 570		ca. 570
Granite Dykes	980 ± 13					
Porphyritic Granite Dyke	1011 ± 8					
Zircon Overgrowths (Rims)	1081 ± 4	1061 ± 14	1035 ± 21	ca. 1070	1061 ± 56	ca. 1080
Migmatite Augen Gneiss	1074 ± 11	1103 ± 13		1104 ± 8	1096 ± 8.4	1076 ± 14
Grey Migmalite Gneiss					1115 ± 12	
Augen Gneiss		1127 ± 12		1124 ± 11	1123 ± 21	
Migmatite Augen Gneiss					1137 ± 14	
Granite Gneiss	1134 ± 11	1131 ± 25		1133 ± 16 1163 ± 6 1130 ± 19		1130 ± 12
Grev Gneiss/Zircon Cores	1143 ± 11	1139 ± 12	1132 ± 16	ca. 1140	1142 ± 21	

144 morphism have been reported from throughout the Maud
145 Belt. These ages were obtained from metamorphic zircon
146 overgrowths in the Heimefrontfjella (Arndt et al., 1991;
147 Jacobs et al., 2003a), Kirwanveggen (Harris et al., 1995;
148 Jackson, 1999), H.U. Sverdrupfjella (Board et al., in press),
149 Gjelsvikfjella (Paulsson and Austrheim, 2003; Bismath
150 et al., 2004) and in central Dronning Maud Land (Jacobs
151 et al., 1998).

152 Grantham et al. (1995) provided a structural summary
153 for the rocks in the H.U. Sverdrupfjella and Kirwanveggen
154 areas and suggested that groups of kinematically equiva-
155 lent structures are present in both areas. They proposed
156 three deformation episodes (D_1 – D_3), with late Mesoproter-
157 ozoic isoclinal folding and penetrative fabric development
158 (D_1) followed by regional warping (D_2) associated with the
159 intrusion of post-tectonic (relative to D_1) dykes and plu-
160 tons (Brattskarvet Suite). Finally, brittle fractures and nor-
161 mal faults (D_3) have been related to the break-up of
162 Gondwana at approximately 170 Ma.

163 Post-tectonic intrusions of mafic composition have been
164 reported from Gjelsvikfjella (Ohta et al., 1990) and from
165 central Dronning Maud Land (Jacobs et al., 2003c). The
166 youngest post-tectonic intrusions include the Brattskarvet
167 Suite dated at 489 ± 10 Ma (C. Jackson, unpublished data)
168 in the H.U. Sverdrupfjella area, a syenite body dated at
169 501 ± 10 Ma (Paulsson and Austrheim, 2003) in the
170 Gjelsvikfjella area and aplite dykes at ca. 480–490 Ma that
171 occur throughout the Maud Belt (Harris et al., 1995; Paul-
172 son and Austrheim, 2003; Jacobs et al., 2003b; Bismath
173 et al., 2004; Board et al., in press).

174 The Maud Belt records three metamorphic episodes
175 (M_1 – M_3), with the first (M_1) being characterized by a gran-
176 ulite-facies mineral assemblage for which P – T conditions
177 of 9–11 kbar and 750–880 °C have been estimated (Groene-
178 wald and Hunter, 1991). A subsequent high-pressure meta-
179 morphic phase (M_{2a}) was distinguished with a minimum
180 pressures estimate of 9 kbar and temperature estimates of
181 between 720 and 850 °C in northern Kirwanveggen (Fer-
182 rar, 1995; Harris, 1999), in western H.U. Sverdrupfjella
183 (Grantham et al., 1995) and in the eastern H.U. Sverdrupfj-
184 ella (Grantham et al., 1995; Groenewald et al., 1995). This
185 was followed by isothermal decompression to conditions
186 transitional between amphibolite and granulite facies
187 ($P = 5$ – 8 kbar; $T = 600$ – 790 °C), which constitutes M_{2b}
188 (Board et al., in press). M_{2c} is distinguished by the growth
189 of biotite laths that have identical chemical composition to
190 that of the fabric-defining syn- D_2 biotite laths implying
191 that M_{2c} evolved directly from M_{2b} , with metamorphism
192 outlasting the main pulse of deformation (Board et al., in
193 press). According to these authors, the mica development
194 most likely reflects regional K-metasomatism related to
195 post-orogenic felsic magmatism. Finally, M_3 is a regional
196 retrograde metamorphic event characterized by the forma-
197 tion of chlorite rims on biotite and the formation of epi-
198 dote, and this has been ascribed to the break-up of
199 Gondwana. Coeval with the break-up of Gondwana is

the emplacement of Jurassic-aged dolerite dykes (Grantham et al., 1995). 200
201

3. Geology of Gjelsvikfjella 202

The rocks of the Gjelsvikfjella area comprise polyde- 203
formed, upper amphibolite-facies gneisses derived from a 204
supracrustal sequence that was intruded by various plu- 205
tonic and hypabyssal bodies. The majority of the rock 206
types in the area are felsic para- and orthogneiss, semipe- 207
litic and pelitic gneiss and metamafic rocks. The felsic rocks 208
have been migmatized to various degrees with the main 209
pulse of migmatization being syn- to post-tectonic (relative 210
to D_2). 211

Five mapable units have been recognized in the 212
Gjelsvikfjella area (Fig. 2). The oldest unit is a metasupra- 213
crustal sequence (referred to here as the Gneiss Complex). 214
The Gneiss Complex is dominated by biotite–garnet gneiss 215
that occurs as concordant layers alternating with felsic and 216
mafic gneisses of variable composition. The biotite–garnet 217
gneiss contains sillimanite, in places with garnet porphyro- 218
blasts, and syn-kinematic biotite that defines S_2 . Two vari- 219
eties of pre-tectonic mafic bodies are present in the 220
Gjelsvikfjella area. The first variety occurs as mafic lenses 221
and boudins of metabasalt and metagabbro, consists of 222
hornblende and plagioclase, and occurs at different tec- 223
tonostratigraphic levels in the Gneiss Complex. The mafic 224
bodies are variably foliated with locally unfoliated garnet 225
amphibolite cores within larger boudins. These cores are 226
in most cases completely surrounded by hornblende and 227
plagioclase. The garnet amphibolite cores consist of garnet, 228
hornblende (mostly as pseudomorphs after clinopyroxene), 229
plagioclase and biotite with minor amounts of quartz, 230
ilmenite, rutile and titanite. The second type is garnet-free 231
amphibolite, which most likely represent re-equilibrated 232
garnet amphibolites rather than mafic rocks of different 233
composition. The garnet-free amphibolite bodies consist 234
of hornblende, plagioclase and biotite with minor amounts 235
of ilmenite, rutile and titanite. Biotite is typically post-tec- 236
tonic and occurs as randomly orientated laths. 237

A third variety of pre-tectonic mafic rock is present east 238
of Gjelsvikfjella. It consists of garnet, hornblende (mostly 239
as pseudomorphs after orthopyroxene), plagioclase and 240
biotite with minor amounts of quartz, ilmenite, rutile and 241
titanite. 242

No evidence of a basement to the above supracrustal 243
sequences has been discovered so far. The oldest plutonic 244
rocks are variably migmatized, medium- to coarse-grained 245
granitic and tonalitic augen gneisses, collectively mapped 246
as Migmatite Gneiss. The leucosome domains therein are 247
strongly deformed and thus contrast with the youngest 248
intrusions, which are post-tectonic felsic and mafic dykes 249
(Fig. 3A and B) and stocks. 250

The Gjelsvikfjella area is distinguished from western 251
Dronning Maud Land by the abundance of post-tectonic 252
mafic dykes (Fig. 3C). These dykes experienced lower 253
amphibolite- to greenschist-facies metamorphism, are med- 254

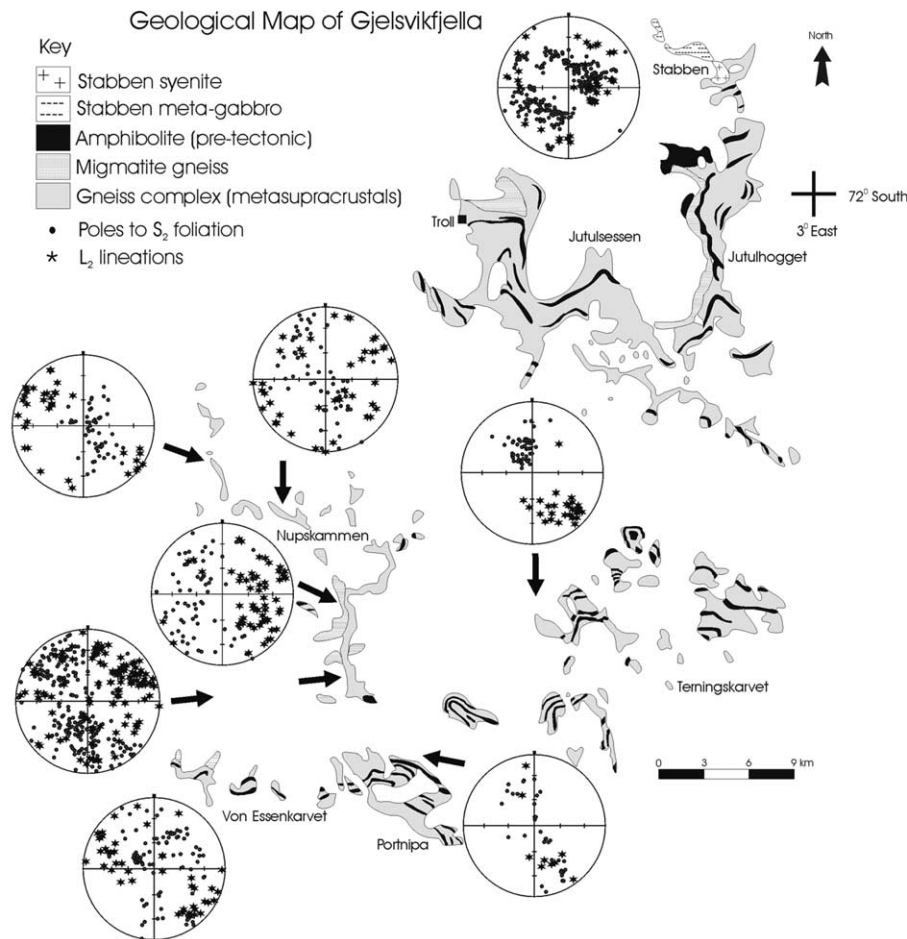


Fig. 2. Geological map of Gjelsvikfjella area (modified after Ohta, 1999), also shown are sample localities and equal-area stereographic projections of L_2 lineations and poles to S_2 foliation.

255 ium- to coarse-grained, melanocratic, hornblende-biotite
 256 rocks with no preferred orientation of the constituent min-
 257 erals. In the northern sector of the study occurs a meta-
 258 gabbro body (Stabben gabbro; Fig. 2). This gabbro is made
 259 up of secondary hornblende, altered brown augite, brown
 260 biotite, relics of clinopyroxene and plagioclase (andesine-
 261 oligoclase). A second, light brown biotite generation is also
 262 present that overgrew the brown biotite. A coarse-grained
 263 variety of the Stabben meta-gabbro contains a greater per-
 264 centage of clinopyroxene and olivine. Accessory phases
 265 present are apatite, titanite and zircon. Preliminary geo-
 266 chemical analyses indicate that the post-tectonic mafic
 267 dykes and the Stabben meta-gabbro share very similar
 268 major and trace element distributions as well as similar
 269 and isotopic composition from which derivation from sim-
 270 ilar mantle sources is inferred. The Stabben meta-gabbro is
 271 intruded by a undeformed post-tectonic syenite body that
 272 is bound to the south by metasupracrustal rocks of the
 273 Gneiss Complex (Figs. 2 and 3D).

274 Primary structures in the rocks of Gjelsvikfjella have
 275 been largely obliterated during metamorphism and mag-
 276 matism. Five deformation events (D_1 – D_5) are recognized.
 277 Relict structures of the first foliation are preserved in mafic

278 boudins. Rootless isoclinal folds are interpreted to repre-
 279 sent F_2 folds. Earlier F_1 folds are difficult to identify,
 280 because these folds were re-orientated during D_2 leading
 281 to type-3 fold interference patterns (after Ramsay, 1967).
 282 This implies continual coaxial refolding of earlier D_1 struc-
 283 tures. These F_2 folds have been rotated so that the fold axes
 284 now plunge parallel to sub-parallel to the dip direction of
 285 the regional pervasive foliation (S_2), i.e. they have a
 286 reclined attitude (Fig. 3E). The dominant S_2 fabric is par-
 287 allel to lithological contacts (Fig. 3A and E) and is defined
 288 by compositional banding on a centimetre- to metre-scale.
 289 The third fabric (S_3) is an axial planar fabric (Fig. 3F),
 290 which is preserved as leucosome domains that parallel the
 291 F_3 fold axial planes. A fourth deformation event (D_4) is
 292 preserved as broad open folds or regional scale warping.
 293 The youngest deformation (D_5) caused vertical to sub-ver-
 294 tical fractures that are parallel to post-tectonic dolerite
 295 intrusions related to Gondwana break-up (Grantham
 296 et al., 1995).

297 Geochronological studies in Gjelsvikfjella (Bisnath
 298 et al., 2004) made it possible to differentiate between a series
 299 of magmatic and metamorphic events. The oldest event
 300 recorded is the formation of an extensive, 1140–1130 Ma,

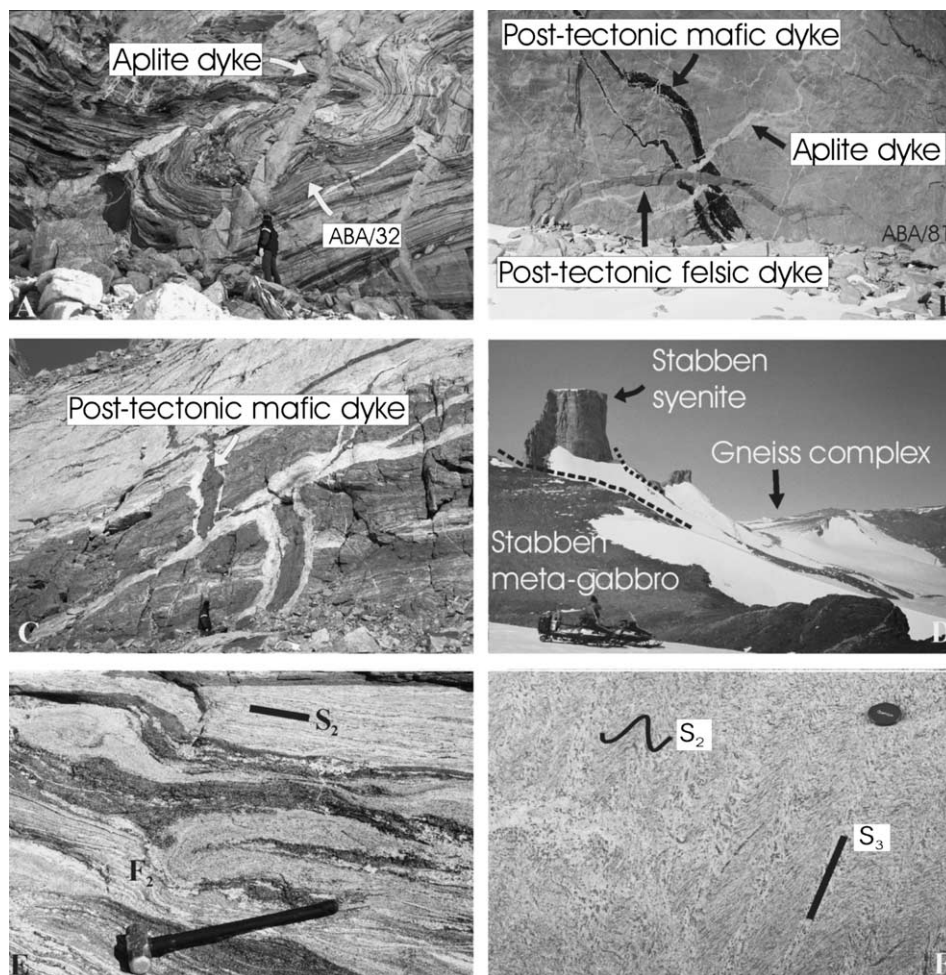


Fig. 3. (A) Post-tectonic aplite dykes; and (B) migmatitic gneiss at Jutulhogget (Fig. 2) also showing post-tectonic dyke relationships; (C) post-tectonic dykes that are discordant to the regional foliation; (D) intrusive relationships (--- intrusive contacts) around Stabben; (E) rootless isoclinal folds showing an early deformation event; (F) Jutulhogget migmatitic gneiss containing leucosomes that are parallel to the axial plane of F_3 folds.

301 volcanic arc. This was followed by 1104 ± 8 Ma granitoids
 302 that might represent, together with so far undated mafic
 303 dykes part of a decompression melting-related bimodal
 304 suite. The first high-grade metamorphism in Gjelsvikfjella
 305 is constrained at approximately 1070 Ma. Intense rework-
 306 ing during the early Cambrian is indicated by ductile refo-
 307 liation, further high-grade metamorphic recrystallization
 308 and metamorphic zircon overgrowths at approximately
 309 530 Ma. This was followed by late- to post-tectonic mag-
 310 matism, reflected by undeformed syenite and gabbro
 311 bodies as well as numerous aplite dykes (498 ± 5 Ma; Bis-
 312 nath et al., 2004). Although the syenite is intrusive into the
 313 gabbro body, it yielded an older Pb–Pb single zircon age of
 314 501 ± 10 Ma (Paulsson and Austrheim, 2003) as opposed
 315 to a SHRIMP U–Pb zircon age of 487 ± 4 Ma (Bisnath
 316 et al., 2004) and SHRIMP U–Pb titanite age of
 317 483 ± 11 Ma (Jacobs et al., 2003b) for the gabbro. This dis-
 318 crepancy between field relationships and geochronological
 319 data is explained by the Pb–Pb age reported for the rela-
 320 tively younger syenite having been obtained by the evapo-
 321 ration technique and possibly including remnants of an
 322 older, inherited zircon component.

4. Metamorphic history

323

The felsic and semipelitic gneiss is dominated by feld- 324
 spar, quartz, biotite and garnet with occasional presence 325
 of hornblende (Table 3). The pelitic gneiss consists of gar- 326
 net, biotite, sillimanite, feldspar and quartz. These mineral 327
 assemblages provide only limited constraints on the meta- 328
 morphic conditions and evolution. More useful in this 329
 regard are the metamafic rocks, which consist of garnet, 330
 clino- and orthopyroxene, plagioclase, hornblende, and 331

Table 3
 Peak metamorphic mineral assemblages identified in the different rock types from Gjelsvikfjella

Rock type	Peak metamorphic mineral assemblage
Felsic paragneiss	Qtz–Kfs–Pl–Bt–Grt–Hbl
Felsic orthogneiss	Qtz–Kfs–Pl–Bt
Metapelitic gneiss	Grt–Sil–Bt–Pl–Kfs–Qtz
Metamafic rock	Hbl–Pl–Ilm–Ttn \pm Rt \pm Grt \pm Qtz \pm Opx Hbl–Pl–Ilm–Ttn \pm Rt \pm Grt \pm Qtz \pm Opx (east of study area)

Mineral abbreviations from Kretz (1983).

Table 4

Representative electron microprobe analyses of garnet (Grt), plagioclase (Plg), orthopyroxene (Opx) and ilmenite (Ilm) for pre-tectonic mafic rocks

Sample	ST/21						ABA/46							
Locality	71°57.90'S, 3°14.38'E						71°57.90'S, 3°14.38'E							
Rock	Garnet-clinopyroxene (relics) amphibolite dyke						Garnet-clinopyroxene (relics) amphibolite dyke							
Grain#	Plg 1	Plg 4	Grt A core	Grt 1 rim	Grt 1 core	Ilm 5	Plg 7	Plg 11	Grt 2 core	Grt 2 rim	Grt 3 rim	Grt 3 core	Ilm 2	Ilm 5
SiO ₂	60.86	56.93	38.91	38.84	38.59	0.05	52.31	59.27	39.03	38.42	38.44	37.82	0.00	0.01
TiO ₂	0.00	0.05	0.09	0.03	0.08	52.46	0.00	0.02	0.03	0.04	0.08	0.00	51.95	51.93
Al ₂ O ₃	25.88	27.68	21.30	21.50	20.81	0.05	28.52	24.98	21.66	21.54	21.43	21.13	0.03	0.00
FeO	0.03	0.11	26.33	29.14	26.60	46.05	0.02	0.14	26.66	27.92	27.13	27.84	46.77	46.78
MnO	0.00	0.03	0.69	1.43	0.97	0.59	0.02	0.00	1.04	1.45	1.26	0.96	0.89	0.87
MgO	0.00	0.00	4.63	3.36	3.90	0.30	0.01	0.01	3.93	3.54	3.31	3.89	0.11	0.07
CaO	7.65	9.65	8.75	7.17	8.78	0.01	11.53	7.40	8.97	8.08	8.85	7.31	0.02	0.00
Na ₂ O	6.62	5.56	0.05	0.10	0.04	0.02	4.39	6.77	0.05	0.00	0.02	0.03	0.00	0.02
K ₂ O	0.21	0.15	0.01	0.04	0.00	0.03	0.03	0.06	0.04	0.00	0.00	0.00	0.00	0.02
Cr ₂ O ₃	0.00	0.00	0.04	0.07	0.00	0.02	0.00	0.00	0.00	0.02	0.00	0.00	0.00	0.00
NiO	0.03	0.00	0.01	0.00	0.00	0.00	0.00	0.00	0.00	0.00	0.00	0.00	0.00	0.06
Total	101.28	100.15	100.81	101.67	99.77	99.57	96.83	98.65	101.41	101.01	100.53	98.97	99.76	99.77
Si	2.67	2.55	3.02	3.02	3.04	0.00	2.44	2.67	3.02	3.00	3.01	3.01	0.00	0.00
Ti	0.00	0.00	0.01	0.00	0.00	0.99	0.00	0.00	0.00	0.00	0.00	0.00	0.98	0.98
Al	1.34	1.46	1.95	1.97	1.93	0.00	1.57	1.33	1.98	1.98	1.98	1.98	0.00	0.00
Fe	0.00	0.00	1.71	1.90	1.75	0.99	0.00	0.01	1.73	1.82	1.78	1.85	1.01	1.01
Mn	0.00	0.00	0.05	0.09	0.06	0.01	0.00	0.00	0.07	0.10	0.08	0.06	0.02	0.02
Mg	0.00	0.00	0.54	0.39	0.46	0.01	0.00	0.00	0.45	0.41	0.39	0.46	0.00	0.00
Ca	0.36	0.46	0.73	0.60	0.74	0.00	0.58	0.36	0.74	0.68	0.74	0.62	0.00	0.00
Na	0.56	0.48	0.01	0.01	0.01	0.00	0.40	0.59	0.01	0.00	0.00	0.00	0.00	0.00
K	0.01	0.01	0.00	0.00	0.00	0.00	0.00	0.00	0.00	0.00	0.00	0.00	0.00	0.00
Cr	0.00	0.00	0.00	0.00	0.00	0.00	0.00	0.00	0.00	0.00	0.00	0.00	0.00	0.00
Ni	0.00	0.00	0.00	0.00	0.00	0.00	0.00	0.00	0.00	0.00	0.00	0.00	0.00	0.00
Total	4.95	4.97	8.00	8.00	7.99	2.01	4.98	4.96	8.00	8.00	7.99	8.00	2.02	2.02
Sample	ABA/47						HEF							
Locality	71°57.90'S, 3°14.38'E						71°57.90'S, 3°14.38'E							
Rock	Orthopyroxene-garnet amphibolite boudin						Garnets amphibolite boudin							
Grain#	Plg 1	Plg 5	Grt 6 rim	Grt 7 core	Grt 5 rim	Grt 6 core	Opx 17	Opx 19	Opx 5	Opx 11	Ilm 8	Plg 4	Plg 9	Plg 13
SiO ₂	47.91	47.50	38.32	38.13	37.71	38.25	49.16	49.34	51.67	49.49	0.03	58.11	56.37	55.69
TiO ₂	0.00	0.04	0.00	0.03	0.02	0.09	0.15	0.13	0.05	0.14	53.18	0.00	0.00	0.00
Al ₂ O ₃	32.06	32.79	21.13	21.31	20.77	21.24	0.52	0.58	0.35	1.51	0.02	26.02	25.62	26.06
FeO	0.44	0.32	31.34	31.09	29.93	30.16	37.68	36.57	35.98	34.06	45.62	0.21	0.05	0.12
MnO	0.00	0.03	1.11	1.03	1.02	1.01	0.41	0.38	0.33	0.30	0.36	0.00	0.00	0.00
MgO	0.00	0.01	2.44	2.39	2.23	2.40	10.48	10.78	10.24	11.01	0.03	0.00	0.00	0.00
CaO	16.15	16.84	6.55	6.14	7.71	7.18	0.37	0.41	0.35	1.57	0.01	8.91	8.73	9.65
Na ₂ O	2.27	2.14	0.04	0.00	0.06	0.04	0.02	0.02	0.07	0.14	0.00	6.59	7.04	6.61
K ₂ O	0.06	0.04	0.01	0.02	0.02	0.01	0.02	0.06	0.00	0.07	0.01	0.10	0.12	0.11
Cr ₂ O ₃	0.00	0.00	0.00	0.03	0.01	0.00	0.00	0.02	0.00	0.01	0.00	0.00	0.00	0.00
NiO	0.02	0.00	0.02	0.00	0.00	0.00	0.00	0.00	0.00	0.00	0.00	0.00	0.00	0.00
Total	98.91	99.70	100.95	100.16	99.47	100.37	98.81	98.30	99.04	98.30	99.28	99.94	97.93	98.26
Si	2.22	2.19	3.03	3.03	3.02	3.03	2.00	2.01	2.07	1.99	0.00	2.61	2.59	2.55
Ti	0.00	0.00	0.00	0.00	0.00	0.01	0.00	0.00	0.00	0.00	1.00	0.00	0.00	0.00

Al	1.75	1.78	1.97	2.00	1.96	1.98	0.03	0.03	0.02	0.07	0.00	1.38	1.39	1.41
Fe	0.02	0.01	2.07	2.07	2.01	2.00	1.24	1.28	1.20	1.15	0.98	0.01	0.00	0.00
Mn	0.00	0.00	0.07	0.07	0.07	0.07	0.01	0.01	0.01	0.01	0.01	0.00	0.00	0.00
Mg	0.00	0.00	0.29	0.28	0.27	0.28	0.65	0.64	0.61	0.66	0.00	0.00	0.00	0.00
Ca	0.80	0.83	0.55	0.52	0.66	0.61	0.02	0.02	0.01	0.07	0.00	0.43	0.43	0.47
Na	0.20	0.19	0.01	0.00	0.01	0.01	0.00	0.00	0.01	0.01	0.00	0.57	0.63	0.59
K	0.00	0.00	0.00	0.00	0.00	0.00	0.00	0.00	0.00	0.00	0.00	0.01	0.01	0.01
Cr	0.00	0.00	0.00	0.00	0.00	0.00	0.00	0.00	0.00	0.00	0.00	0.00	0.00	0.00
Ni	0.00	0.00	0.00	0.00	0.00	0.00	0.00	0.00	0.00	0.00	0.00	0.00	0.00	0.00
Total	5.00	5.01	7.99	7.97	8.00	7.98	3.98	3.98	3.93	3.97	2.00	5.00	5.04	5.04

Formulae based on 12 for garnet, 8 for plagioclase, 3 for ilmenite and 6 for orthopyroxene. All Fe reported as FeO.

ilmenite. These rocks form resistant tectonic lenses and boudins in which much of the metamorphic history is preserved. As these rocks are considered to be intrusive into the paragneiss sequence it is implicit that the host-rock sequence experienced the entire metamorphic history recorded in the metamafic rocks. Given the degree of re-equilibration of the host-rock, any sequence of metamorphic events prior the emplacement of the mafic rocks is probably no longer preserved. Therefore, the pre-tectonic mafic bodies are the most suitable rock type for reconstructing the metamorphic history of the Gjelsvikfjella area.

5. Mineral chemistry

Seven amphibolite samples representing the range of different pre-tectonic mafic rock types in the Gjelsvikfjella area and four samples containing syn-tectonic (with respect to D₂) and post-tectonic biotite laths were selected for mineral chemical analysis (Tables 4 and 5). Mineral chemical data were acquired by conventional microprobe analyses using a JEOL JXA-8800RL electron microprobe at the University of KwaZulu Natal (Westville Campus) equipped with wavelength-dispersive spectrometers and a Cameca Camebax four-channel electron microprobe at the University of Cape Town. The microprobes were run at an accelerating voltage of 15 kV and a beam current of 20 nA and 40 nA on the respective machines. Data reduction by proprietary JEOL ZAF and Cameca PAP correction software, using a range of internationally certified mineral standards were employed. Counting times for peak and background positions were 10 s, with the detection limits for the elements analysed for between 0.02% and 0.09%. Mineral abbreviations used are from Kretz (1983). All Fe is expressed as Fe²⁺ unless otherwise stated.

6. Metamafic rocks

The pre-tectonic metamafic rocks in the Gjelsvikfjella area have been intensely metamorphosed and now consist primarily of hornblende and plagioclase. The cores of these rocks contain evidence of an earlier metamorphic event in the form of coronas of hornblende and plagioclase surrounding garnet and relic clinopyroxene grains. This texture is found in cores of metamafic rocks throughout the Gjelsvikfjella area, regardless of tectonostratigraphic level, therefore implying that the various pre-tectonic mafic bodies record the same polyphase deformational history.

The oldest, poorly preserved mineral assemblage recorded in the pre-tectonic mafic rocks is Grt–Opx–Qtz±Rt. However, orthopyroxene has been observed in two samples (ABA/42 and ABA/47), which were collected from an outcrop east of Stabben (71°57.90'S, 3°14.38'E). The orthopyroxene appears as anhedral grains and, where garnet is present, quartz forms a corona around the garnet (Fig. 4A). Plagioclase in these two samples occurs as sec-

Table 5
Representative electron microprobe analyses of hornblende (Hbl) and biotite (Bio) for pre-tectonic mafic and metapelitic rocks

Sample:	ST/21		ABA/46		ABA/47		HEF			
Grain#:	Hbl 1	Hbl 4	Hbl 7	Hbl 11	Hbl 1	Hbl 5	Hbl 4	Hbl 9	Hbl 13	
SiO ₂	45.62	44.66	42.73	41.01	44.13	43.76	43.01	43.08	44.11	
TiO ₂	1.53	1.52	1.40	1.57	1.39	1.65	1.60	1.28	1.35	
Al ₂ O ₃	9.13	9.98	11.94	14.19	10.67	9.34	12.52	11.14	12.23	
Cr ₂ O ₃	0.02	0.04	0.00	0.00	0.00	0.01	0.00	0.00	0.00	
FeO	20.54	19.81	18.37	17.49	21.27	22.86	22.23	23.33	22.26	
MnO	0.27	0.21	0.26	0.16	0.13	0.13	0.25	0.24	0.26	
MgO	8.94	8.65	8.96	8.17	7.14	7.24	6.67	7.45	6.95	
CaO	10.61	10.82	10.65	11.01	11.28	9.68	11.23	10.36	11.39	
Na ₂ O	1.50	1.33	1.96	1.96	1.18	1.08	1.39	1.33	1.30	
K ₂ O	0.55	0.70	0.67	0.74	0.64	0.67	0.70	0.63	0.60	
NiO	0.03	0.05	0.03	0.00	0.00	0.02	0.00	0.00	0.00	
Total	98.73	97.76	96.97	96.29	97.84	96.43	99.60	98.84	100.44	
Si	6.72	6.65	6.40	6.21	6.65	6.61	6.37	6.36	6.46	
Al(iv)	1.28	1.35	1.60	1.79	1.35	1.39	1.63	1.64	1.54	
T	8	8	8	8	8	8	8	8	8	
Al(vi)	0.30	0.40	0.51	0.74	0.54	0.28	0.56	0.30	0.57	
Ti	0.17	0.17	0.16	0.18	0.16	0.19	0.18	0.14	0.15	
Cr	0.00	0.01	0.00	0.00	0.00	0.00	0.00	0.00	0.00	
Fe(iii)	0.77	0.63	0.67	0.40	0.39	1.16	0.61	1.27	0.61	
Fe(ii)	1.76	1.84	1.63	1.82	2.29	1.73	2.14	1.61	2.12	
Mn	0.03	0.03	0.03	0.02	0.02	0.02	0.03	0.03	0.03	
Mg	1.96	1.92	2.00	1.84	1.60	1.63	1.47	1.64	1.52	
C	5	5	5	5	5	5	5	5	5	
Ca	1.67	1.73	1.71	1.79	1.82	1.57	1.78	1.64	1.79	
Na	0.33	0.27	0.29	0.21	0.18	0.32	0.22	0.36	0.21	
B	2	2	2	2	2	2	2	2	2	
Na	0.10	0.11	0.28	0.36	0.17	0.00	0.18	0.02	0.16	
K	0.10	0.13	0.13	0.14	0.12	0.13	0.13	0.12	0.11	
A	0.20	0.24	0.40	0.50	0.29	0.13	0.31	0.14	0.27	
Total	15.20	15.24	15.40	15.50	15.29	15.01	15.31	15.14	15.27	
	ABA/17			ABA/41			ABA/61			
	Bio 1 syn	Bio 3 syn	Bio 4 ran	Bio 6 ran	Bio 1 syn	Bio 5 syn	Bio 12 ran	Bio 13 ran	Bio 4 syn	Bio 6 ran
SiO ₂	35.59	35.64	34.75	35.92	35.63	35.18	34.89	34.93	36.41	35.60
TiO ₂	3.10	3.02	2.85	2.74	4.28	4.57	2.97	3.70	4.90	4.89
Al ₂ O ₃	15.10	15.15	14.96	15.44	14.85	14.87	15.37	15.17	13.59	13.26
FeO	23.52	23.69	23.39	23.43	25.34	24.48	25.21	24.97	18.37	18.19
MnO	0.05	0.11	0.07	0.06	0.12	0.10	0.11	0.09	0.14	0.08
MgO	8.20	8.23	8.06	8.41	6.69	6.56	7.00	6.71	11.13	10.63
CaO	0.01	0.05	0.23	0.12	0.00	0.01	0.01	0.11	0.00	0.04
Na ₂ O	0.14	0.14	0.14	0.11	0.11	0.17	0.17	0.16	0.11	0.14
K ₂ O	8.82	8.52	8.26	8.19	8.76	8.63	8.44	8.35	9.31	9.20
Cr ₂ O ₃	0.01	0.03	0.03	0.00	0.02	0.00	0.00	0.02	0.00	0.04
NiO	0.04	0.00	0.02	0.00	0.00	0.00	0.00	0.07	0.01	0.01
Total	94.57	94.59	92.76	94.41	95.79	94.57	94.17	94.28	93.97	92.08
Si	6.09	6.09	6.06	6.12	6.07	6.05	6.04	6.04	6.14	6.14
Al	1.91	1.91	1.94	1.88	1.93	1.95	1.96	1.96	1.86	1.86
T-site	8.00	8.00	8.00	8.00	8.00	8.00	8.00	8.00	8.00	8.00
Al	1.14	1.14	1.14	1.22	1.05	1.07	1.18	1.13	0.84	0.83
Ti	0.40	0.39	0.37	0.35	0.55	0.59	0.39	0.48	0.62	0.63
Fe(ii)	3.37	3.39	3.41	3.34	3.61	3.52	3.65	3.61	2.59	2.62
Cr	0.00	0.00	0.00	0.00	0.00	0.00	0.00	0.00	0.00	0.01
Mn	0.01	0.02	0.01	0.01	0.02	0.01	0.02	0.01	0.02	0.01
Mg	2.09	2.10	2.10	2.14	1.70	1.68	1.81	1.73	2.80	2.73
O-site	7.00	7.03	7.04	7.05	6.92	6.87	7.04	6.97	6.87	6.84
Ca	0.00	0.01	0.04	0.02	0.00	0.00	0.00	0.02	0.00	0.01
Na	0.05	0.05	0.05	0.04	0.04	0.06	0.06	0.05	0.04	0.05
K	1.93	1.86	1.84	1.78	1.90	1.89	1.86	1.84	2.00	2.02
A-site	1.97	1.91	1.93	1.84	1.94	1.95	1.92	1.92	2.04	2.08
Total	16.97	16.94	16.97	16.89	16.86	16.83	16.96	16.88	16.91	16.92

Formulae based on 23 oxygens for hornblende and 24 (O+OH) for biotite. All Fe reported as FeO.

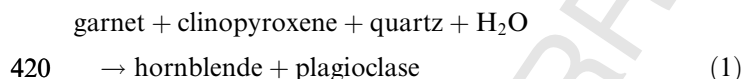
Note: syn = biotite parallel to S2; ran = randomly oriented biotite.

385 ondary, interstitial grains. This initial assemblage re-equil-
386 ibrated during subsequent metamorphism and is now dom-
387 inated by Hbl–Pl–Ilm±Ttn (Fig. 4B).

388 Another poorly preserved mineral assemblage recorded
389 in pre-tectonic mafic rocks is Grt–Cpx–Qtz±Rt. This
390 assemblage re-equilibrated subsequently, which led to the
391 widespread development of the dominant mineral assem-
392 blage Hbl–Pl–Ilm±Ttn (Fig. 4B) in the entire study area,
393 with only few relics of the original assemblage being pre-
394 served. Clinopyroxene is rarely observed but mainly
395 inferred from the presence of pseudomorphs of hornblende
396 (Fig. 4C). Where garnet is preserved, it contains inclusions
397 of rutile and, in places, quartz, with a corona of plagioclase
398 around the garnet.

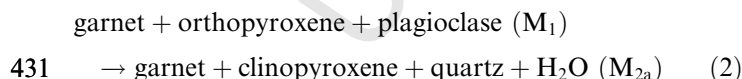
399 Hornblende (0.1–5 mm in size) and plagioclase (1–
400 3.5 mm in size) are the dominant minerals and typically
401 occur as symplectitic intergrowths where they form corona
402 structures around earlier formed pyroxene. As matrix con-
403 stituent they display a granoblastic texture. Rutile and
404 ilmenite occur both within the matrix and as inclusions in
405 hornblende. Titanite is in textural equilibrium with the
406 hornblende. The regional pervasive fabric (S_2) in the foli-
407 ated parts of the pre-tectonic metamafic rocks is defined
408 by hornblende and plagioclase with inclusions of ilmenite
409 and titanite in the hornblende indicating that the formation
410 of these minerals occurred syn- D_2 .

411 The granulite-facies Grt–Opx–Qtz±Rt assemblage was
412 also noted in the H.U. Sverdrupfjella, where Groenewald
413 and Hunter (1991) ascribed it to M_1 . Recent petrological
414 and textural studies on the rocks from that area (Board
415 et al., in press) revealed decompression of a Grt–Cpx–
416 Qtz±Rt assemblage from eclogite-facies (M_{2a}) to upper
417 amphibolite-facies (M_{2b}) conditions by the continuous
418 reaction



421 However, in Gjelsvikfjella only relics of the M_{2a} assem-
422 blage could be observed and the syn- M_{2b} Hbl–Pl–Ilm±Ttn
423 assemblage dominates.

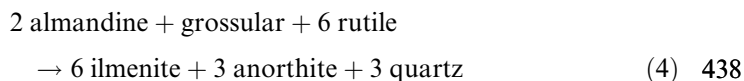
424 Samples ABA/42 and ABA/47 from east of Gjelsvikfj-
425 ella show petrological and textural relationships that point
426 to decompression to upper amphibolite-facies (M_{2b}) condi-
427 tions. The Opx–Grt assemblage is regarded as syn- M_1 and
428 is assumed to have reacted to the Cpx–Grt assemblage by
429 the reaction



432 the products of which, in turn, broke down by the reaction
433 garnet + clinopyroxene + quartz + H_2O



435 The distribution of rutile and ilmenite between the garnet
436 and matrix indicates the net-transfer reaction



439 All of the plagioclase occurs as secondary (M_{2b}) reaction
440 product that typically forms coronas around garnet grains.
441 No associated penetrative fabric can be assigned to the M_{2a}
442 mineral assemblage, therefore suggesting that the M_{2a} min-
443 eral assemblage has a pre- D_2 origin, although the lack of a
444 fabric could be simply due to the competent nature of the
445 mafic bodies making such rocks more resistant to deforma-
446 tion than the host paragneisses and metavolcanic rocks.

447 Widely spaced biotite laths (Fig. 4D) that are aligned
448 parallel to the S_2 fabric cut across the M_{2a} and M_{2b} mineral
449 assemblages. The abundance of biotite increases from the
450 cores ($\ll 1$ vol.%) to the margins (20–25 vol.%) of the mafic
451 bodies. This distribution suggests that biotite formation
452 was probably related to potassic fluid flow during a retro-
453 grade metamorphic event (M_{2c}). Some biotite grains,
454 together with hornblende, define the S_2 fabric, whereas oth-
455 ers are randomly orientated (Fig. 4D). As the two textural
456 types of biotite do not differ in their composition, it is
457 inferred that M_{2c} may have started during D_2 but outlasted
458 that deformation event.

459 No fabric/mineral assemblage-forming event has been
460 recognized to be associated with D_3 . A final metamorphic
461 event (M_3) is expressed by the local retrograde alteration
462 of biotite to chlorite.

463 A total of 443 electron microprobe analyses were con-
464 ducted on garnet, orthopyroxene, plagioclase, ilmenite,
465 amphibole and biotite. Representative mineral analyses
466 for each sample are given in Tables 4 and 5.

467 Garnet makes up between 10 and 50 vol.% of the
468 amphibolites and is almandine-rich ($X_{\text{Alm}} = 40\text{--}68\%$,
469 $X_{\text{Gross}} = 15\text{--}32\%$, $X_{\text{Pyr}} = 9\text{--}29\%$, $X_{\text{Spess}} = 1\text{--}5\%$). The Fe/
470 (Fe + Mg) ratio ranges from 0.56 to 0.84. Garnet profiles
471 for five samples (ST/21, ABA/15, ABA/42, ABA/46 and
472 ABA/47) show flat zonation patterns regardless of the size
473 and orientation of the analysed grain. In some grains
474 (Fig. 5), the X_{Pyr} proportion displays a slight increase from
475 rim to core with a corresponding decrease in X_{Alm} , with
476 X_{Spess} and X_{Gross} remaining constant.

477 Pseudomorphs of clinopyroxene, where present (sam-
478 ples ABA/15, ABA/46 and ST/21), make up 10–25 vol.%,
479 and consist of syn- M_{2b} hornblende. Orthopyroxene (10–
480 20 vol.%) was found in sample ABA/47. It is poor in Al
481 ($\text{Al}_2\text{O}_3 < 1.5$ wt.%) and has an X_{Fe} ratio between 0.57
482 and 0.69 (Fig. 6).

483 Amphibole makes up between 10 and 50 vol.% and it
484 shows little compositional variation. Amphibole grains
485 from sample ABA/15 have a low Fe/(Fe + Mg) ratio
486 (0.30–0.33) compared to those hosted by the other samples
487 in which this ratio ranges from 0.44 to 0.65. Assuming all
488 Fe as Fe^{2+} , the amphibole compositions correspond to
489 magnesiohornblende to tschermakite and pargasite
490 (Fig. 7).

491 Two chemically distinct varieties of plagioclase (modal
492 proportion: 5–45 vol.%) were identified (Fig. 8). The first

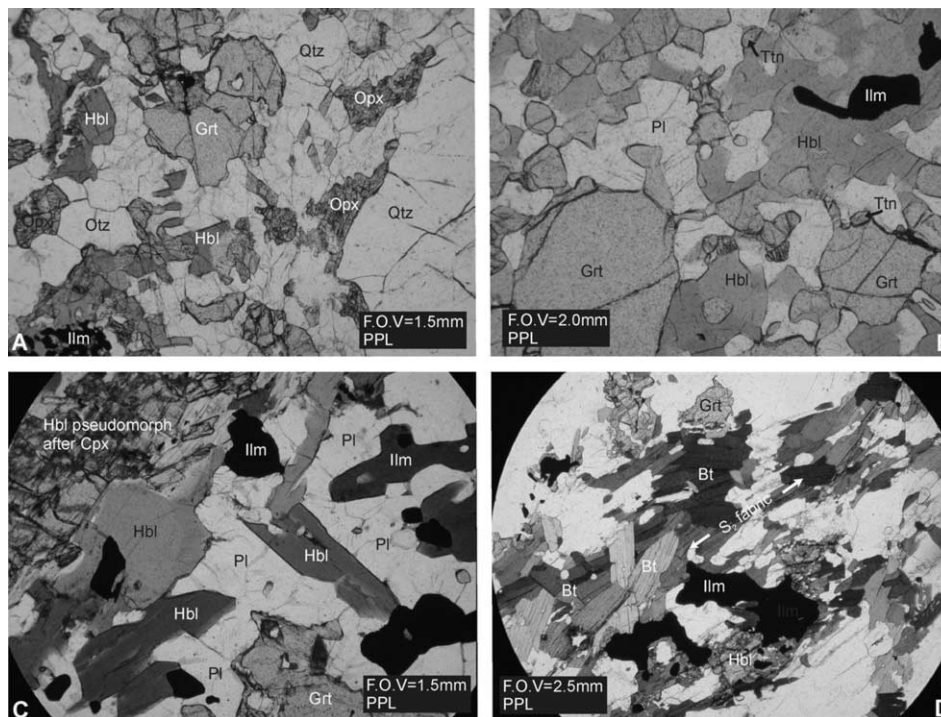


Fig. 4. (A) Syn- M_1 garnet (Grt) and orthopyroxene (Opx), with M_{2b} hornblende (Hbl) and quartz (Qtz), sample ABA/47; (B) syn- M_{2a} garnet surrounded by M_{2b} hornblende, plagioclase (Pl), ilmenite (Ilm) and titanite (Ttn), sample ST/20; (C) syn- M_{2a} garnet and hornblende pseudomorphs after clinopyroxene surrounded by plagioclase, hornblende and inclusion of ilmenite, sample ST/21; (D) syn- M_{2a} garnet with M_{2b} hornblende and syn- to post- M_{2b} biotite laths, sample ABA/61.

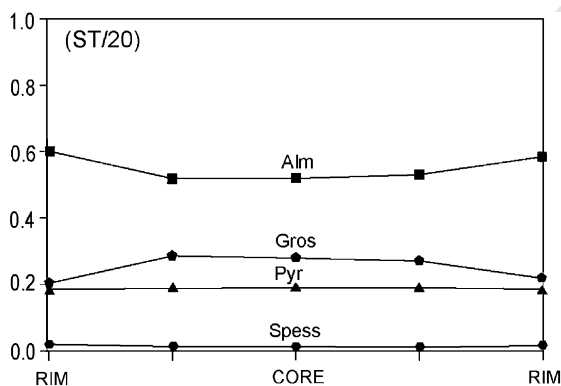


Fig. 5. Representative compositional zoning profiles across individual garnet grains from sample ST/20.

493 group ranges in composition from An_{80} to An_{100} and the
 494 second group has a composition of An_{30} to An_{50} . A few
 495 analyses are scattered between these two chemically distinct
 496 varieties. The orthoclase contents are generally less than
 497 1.25%.

498 7. Geothermobarometry

499 The application of geothermobarometry to the pre-tec-
 500 tonic mafic rocks is complicated due to the polyphase meta-
 501 morphic history. The Opx-Grt geothermometer of Pattison
 502 et al. (2003) was applied to the only orthopyroxene-bearing

sample (ABA/47), which preserves an inferred M_1 assem- 503
 blage. The orthopyroxene and garnet occur in minor modal 504
 proportions and are surrounded by quartz (Fig. 4A) in most 505
 instances. No suitable phase relationships were identified 506
 to assist with the determination of equilibrium pressure 507
 conditions. Assuming a minimum and maximum pressure 508
 of 7 and 10 kbar (by analogy with results obtained from 509
 adjacent areas by Groenewald and Hunter, 1991, and 510
 Bucher-Nurminen and Ohta, 1993), temperatures between 511
 750 and 800 °C were calculated with the RCLC-P pro- 512
 gramme (Pattison et al., 2003; <http://www.petrology.oupjournals.org> or http://www.geo.ucalgary.ca/~pattison/drm_pattison-rclc.htm). This geothermometer is preferred 513
 over previously published calibrations for the Opx-Grt ge- 514
 othermometer, because it takes into account the Al-solubility 515
 in orthopyroxene and also the influence of late Fe-Mg 516
 exchange as a result of closure temperatures below granu- 517
 lite-facies conditions and retrogressive net-transfer reac- 518
 tions (Spear and Florence, 1992; Kohn and Spear, 2000; 519
 Pattison et al., 2003). 520
 521
 522

The M_{2a} mineral assemblage has been largely replaced 523
 by the M_{2b} mineral assemblage. Therefore the composition 524
 of the original syn- M_{2a} garnet has most likely changed as a 525
 result of differences in diffusion rates during high-grade 526
 metamorphism (Yardley, 1991). The preservation of M_{2a} - 527
 clinopyroxene only as hornblende pseudomorphs further 528
 hindered the quantification of M_{2a} -conditions. 529

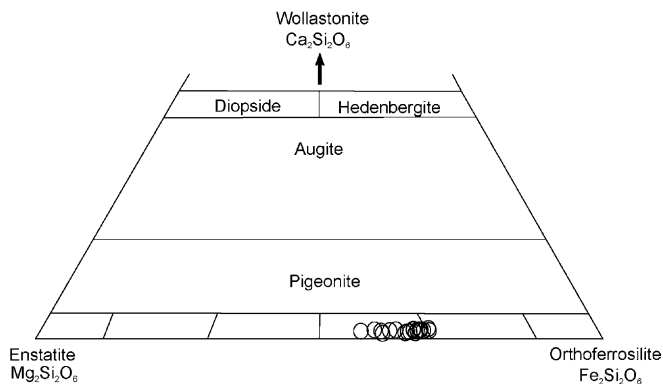


Fig. 6. Classification of Ca-Fe-Mg orthopyroxene in sample ABA/47 according to the scheme of Morimoto (1998).

530 The newly formed hornblende and plagioclase provides
 531 an opportunity of placing constraints on the M_{2b} P - T con-
 532 ditions. To this effect the Hbl-Pl (Holland and Blundy,
 533 1994) and Grt-Hbl geothermometers (Graham and Powell,
 534 1984), and the Grt-Hbl-Pl-Qtz geobarometer (Kohn and

Spear, 1990) were employed. The edenite-tremolite geo-
 thermometer of Holland and Blundy (1994) was applied
 to all samples because of the presence of small amounts
 of quartz. This geothermometer is suitable for a tempera-
 ture range of 500–1100 °C and amphiboles that contain
 <7.8 Si atoms per formula unit, which is the case for the
 samples studied. In each sample, P - T estimates were made
 for several microdomains in which the relevant phases
 appear to be in textural equilibrium.

In all the samples analysed the temperatures calculated
 from Grt-Hbl thermometry are at least 850 °C, which is
 at variance with those obtained from the Hbl-Pl thermom-
 etry (709–785 °C). The latter is preferred as it finds support
 from the abundance of amphibole and the presence of plagioclase
 with compositions between An_{30} and An_{50} . The
 pressures calculated using the Grt-Hbl-Pl-Qtz method of
 Kohn and Spear (1990) for samples ABA/46 and ST/21
 are 6.8 and 6.1 kbar, respectively. Plagioclase in samples
 ABA/46 and ST/21 has a wide range in anorthite content
 ($X_{An} = 0.38$ – 0.72 and 0.38 – 0.46 , respectively). The lower
 X_{An} ratios are most likely a result of partial diffusional

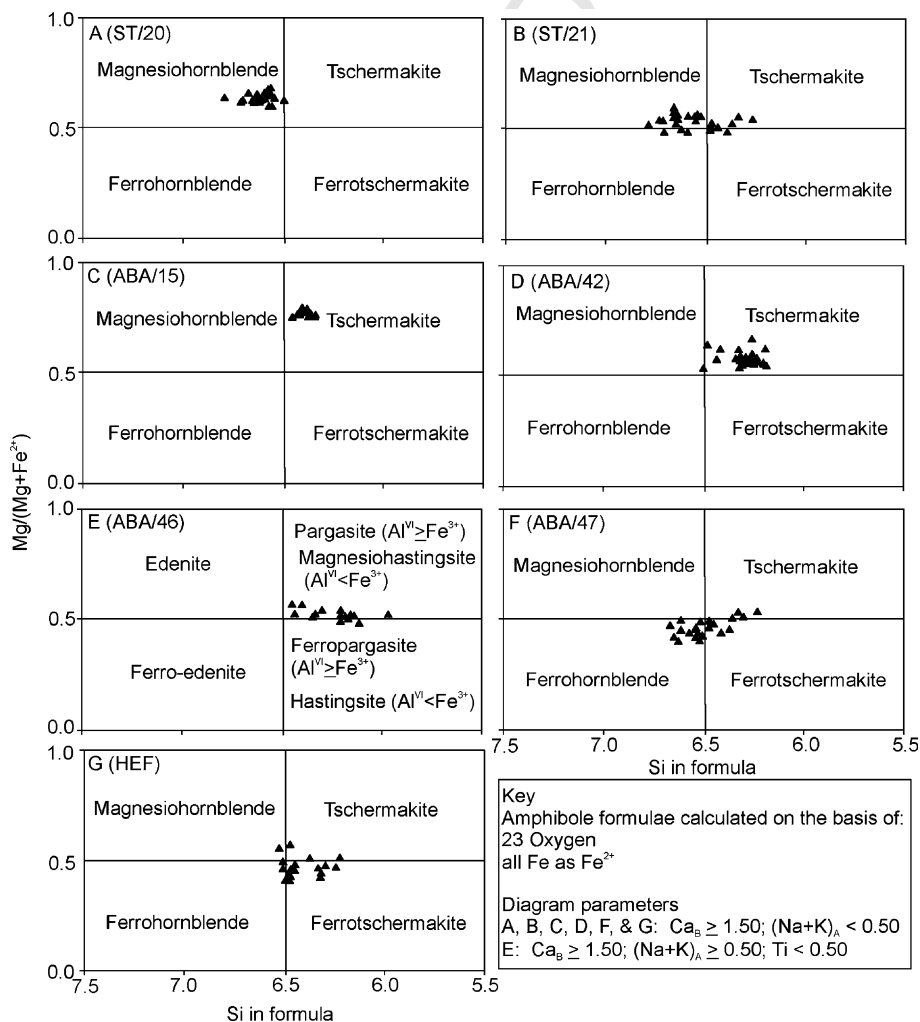


Fig. 7. Amphibole classification for samples: (A) ST/20, (B) ST/21, (C) ABA/15, (D) ABA/42, (E) ABA/46, (F) ABA/46 and (G) HEF, according to the classification scheme of Leake et al. (1987).

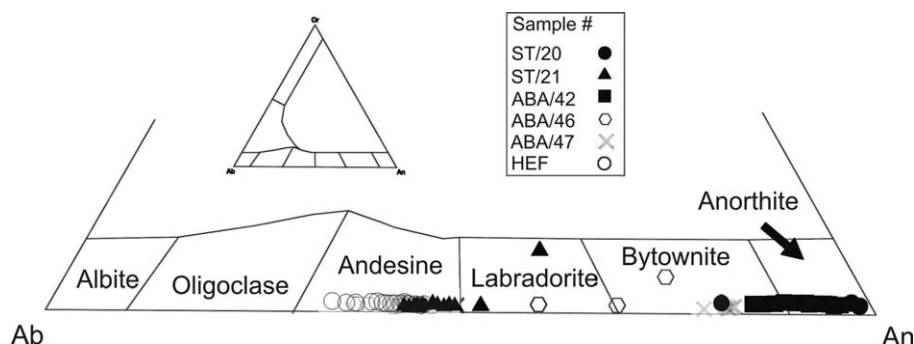


Fig. 8. Composition of plagioclase in pre-tectonic metamafic rocks.

556 resetting during retrograde metamorphism. The higher X_{An}
 557 ratios have been assumed to be least affected by retrograde
 558 metamorphism and were therefore used to calculate M_{2b}
 559 pressure conditions. The use of lower X_{An} ratios in pressure
 560 calculations produced pressure estimates of ≤ 4.8 kbar.
 561 This variation in pressure could also be an artifact of
 562 extrapolation from end-member compositions, bearing in
 563 mind the wide range in $Fe/(Fe + Mg)$ ratio from 0.44 to
 564 0.60 in the hornblende. This range in hornblende composi-
 565 tion is most likely also attributable to diffusional resetting
 566 during retrograde metamorphism. Combining the results
 567 of the various geothermobarometers gives an overall tem-
 568 perature range for M_{2b} of 709–785 °C at a minimum pres-
 569 sure of 6.1 kbar. Textural disequilibrium between biotite
 570 and the earlier formed minerals does not permit the use
 571 of geothermobarometry to quantify M_{2c} P – T conditions.

572 The results of the various geothermobarometers were
 573 compared with those obtained by applying the average P –
 574 T method (Powell and Holland, 1994) to garnet-bearing
 575 amphibolite samples using the program THERMOCALC
 576 version 2.75 (Powell et al., 1998). Mineral analyses from
 577 micro-domains in which all the M_{2b} phases appear to be
 578 in textural equilibrium were selected for optimal geother-
 579 mobarometry, and the activities of the various end-members
 580 were calculated using the program AX ([http://www.esc.
 581 cam.ac.uk/astaff/holland/index.html](http://www.esc.cam.ac.uk/astaff/holland/index.html)). Limited fluid activity
 582 is evident from symplectitic textures (e.g. Messiga et al.,
 583 1990; Board et al., in press). Powell and Holland (1994) sug-
 584 gested that the average fluid composition most likely corre-
 585 sponds to that for which a minimum σ -fit is obtained in
 586 P – T – X calculations. Therefore average P – T estimates were
 587 modeled using different fluid compositions until a minimum
 588 value of σ -fit was obtained, resulting in: $X_{CO_2} = 0.1$ and
 589 $X_{H_2O} = 0.5$. Combining the results of the application of
 590 optimal geothermobarometry to the various samples results
 591 in an overall range in P – T estimates of $T = 638$ – 733 °C and
 592 $P = 7.0$ – 9.5 kbar.

593 8. P – T path

594 Three stages of metamorphic recrystallization can be
 595 distinguished in the studied rocks. The first stage (M_1) is
 596 evident as garnet-orthopyroxene relics within strain-pro-

597 tected boudins. A temperature of formation between 750
 598 and 800 °C was calculated for this stage. Pressure could
 599 not be quantified but only crudely estimated between 7
 600 and 10 kbar.

601 The second stage (M_2) is a series of metamorphic events
 602 that are subdivided into M_{2a} to M_{2c} . Studies by Board et al.
 603 (in press) in an adjacent area have shown that the garnet-
 604 clinopyroxene relics (M_{2a}) record a minimum pressure of
 605 12.9 kbar but no reliable temperature estimate could be
 606 derived for these relics. By analogy, a similar pressure is
 607 inferred for the M_{2a} conditions in Gjelsvikfjella.

608 The dominant mineral assemblage formed during the
 609 second M_2 event (M_{2b}). The P – T conditions calculated
 610 for this event, using the Hbl–Pl thermometer and Grt–
 611 Hbl–Pl–Qtz geobarometer, are subject to large errors due
 612 to a variety of uncertainties (e.g. Spear, 1993; Bucher and
 613 Frey, 1994) that range from: (i) uncertainties in the electron
 614 microprobe standard compositions, correction factors and
 615 analytical imprecision in microprobe analysis; (ii) the accu-
 616 racy of calibration of experiments on which a geother-
 617 mobarometer is based; (iii) problematic Fe^{2+}/Fe^{3+}
 618 estimates; (iv) the cross-correlations between errors in tem-
 619 perature and pressure estimates as they are interdependent;
 620 and (v) uncertainties in the composition-activity models for
 621 the various solid solutions. The M_{2b} P – T estimates for the
 622 metamafic rocks plot between the water-saturated granite
 623 solidus and water-absent muscovite melting reaction in
 624 the NKASH system (White et al., 2001). Furthermore, they
 625 plot on the low temperature side of the wet basalt solidus.
 626 The low fluid activities derived for the pre-tectonic metam-
 627 afic rocks are therefore consistent with the lack of partial
 628 melting in these rocks.

629 The temperature ranges produced using the Hbl–Pl
 630 method of Holland and Blundy (1994) and THERMO-
 631 CALC program of Powell et al. (1998) are between 709–
 632 785 °C and 638–733 °C, respectively. The difference in
 633 calculated temperature could be a result of variable subse-
 634 quent retrograde metamorphism. The minimum pressure
 635 calculated using the method Kohn and Spear (1990) is
 636 similar to that using THERMOCALC and thus the follow-
 637 ing P – T estimates are favoured: $T = 709$ – 785 °C; $P =$
 638 7–9.5 kbar (Fig. 9).

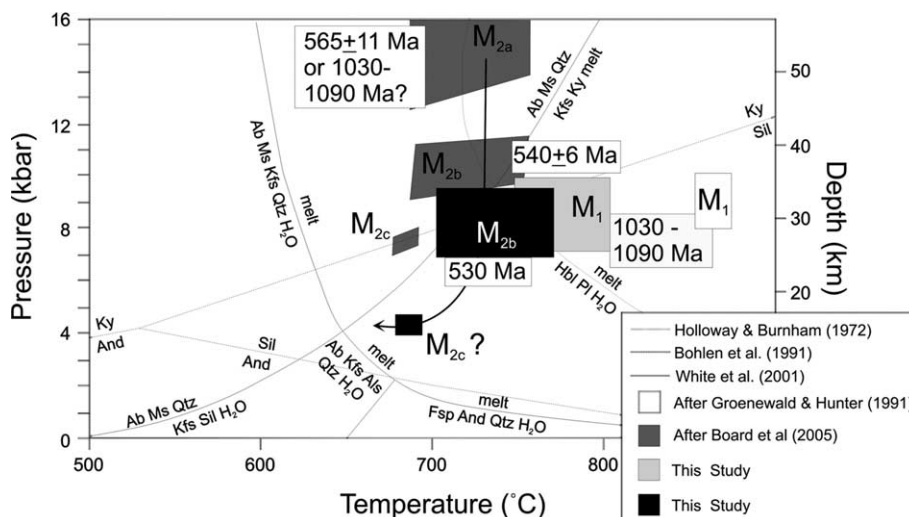


Fig. 9. Suggested pressure–temperature–time path for the pre-tectonic mafic gneiss from Gjelsvikfjella. Al_2SiO_5 equilibria, granitic and basaltic solidus curves shown for reference.

639 The third M_2 event (M_{2c}) is represented by the growth of
 640 biotite in highly variable proportions in most rock types
 641 resulting in a retrograde overprint of the fabric-forming
 642 minerals. Possible P – T conditions for this event
 643 ($T = 677$ – 693 °C; $P = 7.0$ – 8.1 kbar) were calculated by
 644 Board et al. (in press) on kyanite-bearing metapelitic
 645 gneiss. However, in Gjelsvikfjella the pressure is assumed
 646 to be lower (<3 kbar) due to the presence of sillimanite.
 647 The final metamorphic stage (M_3) is represented by the
 648 growth of chlorite on biotite rims.

649 9. Discussion

650 The earliest stage of metamorphism from rocks immedi-
 651 ately east of the main study area reflects granulite-facies
 652 conditions. Geothermometry on an orthopyroxene-gar-
 653 net-bearing mafic granulite gave temperatures between
 654 750 and 800 °C. This temperature range is consistent with
 655 minimum P – T estimates of 750 °C and 8 kbar calculated
 656 for orthopyroxene-garnet gneisses in the area further east
 657 in Mühlig-Hofmannfjella (Bucher-Nurminen and Ohta,
 658 1993) and results obtained on similar rocks further west
 659 in H.U. Sverdrupfjella (Groenewald and Hunter, 1991),
 660 where temperatures and pressures of 750–880 °C and
 661 9–11 kbar were obtained on garnet and orthopyroxene
 662 cores and orthopyroxene–clinopyroxene-garnet coronas,
 663 respectively. By analogy, a similar pressure is assumed
 664 for the orthopyroxene-garnet gneiss in Gjelsvikfjella. This
 665 early metamorphism in the H.U. Sverdrupfjella has been
 666 interpreted to represent a late Mesoproterozoic (M_1) event
 667 (Groenewald and Hunter, 1991), whereas the onset of high-
 668 pressure metamorphism at ca. 565 Ma followed by isother-
 669 mal decompression to upper amphibolite facies has been
 670 ascribed to the Pan-African orogeny (Board et al., in
 671 press). This recently documented Pan-African event in
 672 H.U. Sverdrupfjella has been recognized as the dominant

pervasive fabric forming event and, by analogy, a similar
 Pan-African age is inferred also for Gjelsvikfjella. In
 Mühlig-Hofmannfjella, the orthopyroxene-garnet-bearing
 assemblage could either represent a late Mesoproterozoic
 (M_1) or a late Neoproterozoic/Cambrian metamorphic
 event (Bucher-Nurminen and Ohta, 1993). It could be
 related to the emplacement of late Mesoproterozoic gran-
 ites or to a late Neoproterozoic/Cambrian orogenic cycle
 characterized initially a by a collisional tectonic setting
 and with accompanying crustal thickening resulting in
 granulite facies metamorphism.

Although no reliable age date exist for the orthopyrox-
 ene-bearing rocks from Gjelsvikfjella, a late Mesoproter-
 ozoic age is favoured for the following reasons: (i) The mafic
 rocks studied here are metamorphosed and deformed,
 whereas the orthopyroxene-bearing rocks from central
 Dronning Maud Land are typically late syn- to post-tec-
 tonic leucosomes that cut not only the regional foliation
 but also 535 to 500 Ma charnockite stocks and plutons.
 These leucosomes also contain inclusions of deformed
 mafic rocks that most probably represent disrupted former
 dykes or sills (Engvik and Elvevold, 2004) and possibly the
 equivalents of the mafic rocks studied here. (ii) The dom-
 inant mineral assemblage (i.e. $\text{Hbl} - \text{Pl} - \text{Ilm} \pm \text{Ttn} \pm \text{Rt} \pm \text{Grt} \pm$
 $\text{Cpx} \pm \text{Qtz}$) in the Gjelsvikfjella area is identical to the peak
 metamorphic assemblage and fabric-forming (S_2) minerals
 from the H.U. Sverdrupfjella area for which an early high-
 P event of Pan-African age has been suggested (Board
 et al., in press). By analogy, the same age for the peak
 metamorphic mineral assemblage in the study area is
 inferred. (iii) Evidence of a late Mesoproterozoic high-
 grade metamorphic stage exists in the form of zircon over-
 growths at ca. 1070 Ma (Jacobs et al., 2003d; Bisnath et al.,
 2004; Board et al., in press).

Within the main study area the earliest metamorphic
 stage is represented by a clinopyroxene- and garnet-bear-

ing, plagioclase-free mineral assemblage, which is identical to mineral assemblages recording a presumably early Pan-African eclogite-facies metamorphic event (M_{2a}) in the H.U. Sverdrupfjella (Board et al., in press). A comparable metamorphic stage is also assumed for the rocks in the study area. The M_{2a} event was followed by well constrained regional syn-tectonic amphibolite-facies (M_{2b}) at a temperature between 709 and 785 °C and a pressure between 7 and 9.5 kbar, and retrograde, upper amphibolite-facies post-tectonic metamorphism (M_{2c}) at a pressure of less than 3 kbar. Thus the Pan-African tectono-thermal episode in Gjelsvikfjella followed a clockwise P – T – t path.

The M_{2b} P – T conditions in Gjelsvikfjella area are similar to the P – T conditions calculated for the H.U. Sverdrupfjella area, however, in Gjelsvikfjella the calculated pressure estimates are 2–3 kbar lower than the estimates for H.U. Sverdrupfjella. Considering the top-to-northwest transport direction for the Maud Belt, the Gjelsvikfjella area takes a structurally higher position than the H.U. Sverdrupfjella area, thus explaining the lower pressure experienced during M_{2b} . This decrease in pressure from west to east is further reflected by low- P , high- T rocks reported from Mühlig-Hofmannfjella further east (Bucher-Nurminen and Ohta, 1993; Owada et al., 2003). Paulsson and Austrheim (2003) suggested that a continent–continent collision model with thickening crust and later detachment of the lithospheric root may be applied. This model includes a large heat input from the mantle, extension of crust and removal of subducted material during which the uplift rate of the crust and temperature was high while the pressure decreased as uplift proceeded, leading to late- or post-collisional granitoids and gabbro bodies (Andersen et al., 1991; Paulsson and Austrheim, 2003) on a regional scale, as seen in central Dronning Maud Land.

In Pan-African times, Gjelsvikfjella experienced extensive tectono-thermal overprint of Mesoproterozoic protoliths rather than a purely thermal overprint. This is in good agreement with evidence presented from H.U. Sverdrupfjella further to the west (Board et al., in press) and from the Shackleton Range further south (Talarico et al., 1999) Although no juvenile Pan-African crust has been documented from the Maud Belt, the eclogite relics described in the this study and from H.U. Sverdrupfjella could be an indication of an early Pan-African subduction zone and subsequent continental collision, thereby implying the possible existence of a Neoproterozoic ocean in this sector of East Antarctica.

10. Geodynamic model for the Maud Belt

New data acquired in this study, together with recently published data from other parts of the Maud Belt, make it possible to distinguish a series of tectono-thermal events. Some of the new data are not consistent with previous models for the tectonic evolution along the southern and eastern margins of the Kaapvaal–Grunehogna Craton, particularly during Mesoproterozoic times. Therefore, the

following model (Fig. 10) is proposed from the late Mesoproterozoic to present on the basis of the above discussion and includes the incorporation of geochronological data (Bisnath et al., 2004) and geochemical data (Grosch et al., 2004). The so far oldest rocks from Gjelsvikfjella formed within an approximately 1130 Ma volcanic arc (Bisnath et al., 2004), contemporaneous with arc magmatism along the entire length of the Maud Belt. In previous models (e.g. Groenewald et al., 1995; Jacobs et al., 1993) this arc has been linked with an oceanic island arc to the south of the craton, remnants of which are preserved in the Natal sector of the Namaqua–Natal Belt in South Africa. However, available data from that sector (Cornell et al., 1996; Thomas et al., 1999; Johnston et al., 2001) point to arc magmatism having occurred there some 70 myr earlier. Further west, in the Namaqua sector of that belt, arc magmatism commenced even earlier (Frimmel, 2004). Apart from significant differences in the timing of arc magmatism, different kinematic vectors for the accretion of arc material onto the Kaapvaal–Grunehogna Craton speak against a single, continuous volcanic arc stretching all around the craton from the Namaqua–Natal to the Maud Belt.

For the Natal sector, subduction away from the craton has been suggested to explain the postulated oceanic island arc there (Jacobs and Thomas, 1994; Arima et al., 2001) and, by analogy, a similar outboard direction of subduction has also been suggested for the Maud Belt (Bauer et al., 2003; Basson et al., 2004). Such a model implies a forearc position for the volcano-sedimentary Ritscherflya Supergroup between the Maud Belt and the Grunehogna Craton. The geochemistry of the basin fill points to sediment derivation from an active volcanic arc system (Basson et al., 2004). Magmatic zircon ages of 1131 ± 7 Ma from pyroclastic beds in the lower Ritscherflya Supergroup (Frimmel, 2004) indicate sedimentation to have occurred at the same time as volcanic arc formation. The arc preserved in the Maud Belt is therefore regarded as the main source for the sediments and pyroclastic rocks in the Ritscherflya Basin. Few older, inherited zircon grains in various high-grade metamorphic rocks of the Maud Belt have been recorded in Gjelsvikfjella (Bisnath et al., 2004), H.U. Sverdrupfjella (Board et al., in press), Heimefrontfjella (Arndt et al., 1991; Jacobs et al., 1996) and in the northern Kirwanveggen (Harris, 1999), ranging from 1200 to 2100 Ma. Their existence, together with Nd model ages as old as Archaen (E. Grosch and A. Bisnath, unpublished data), indicate that the Maud arc was not an oceanic island arc but formed adjacent to an Archean Craton, presumably the Grunehogna Craton. Consequently, the direction of subduction that led to the formation of the Maud arc is suggested to have been inboard beneath the Kaapvaal–Grunehogna Craton (Fig. 10A).

Following arc magmatism, a further magmatic pulse at approximately 1100 Ma produced phenocrystic granite bodies (now present as augen gneiss)—not only in Gjelsvikfjella (Bisnath et al., 2004) but on a subcontinental

764
765
766
767
768
769
770
771
772
773
774
775
776
777
778
779
780
781
782
783
784
785
786
787
788
789
790
791
792
793
794
795
796
797
798
799
800
801
802
803
804
805
806
807
808
809
810
811
812
813
814
815
816
817
818
819
820

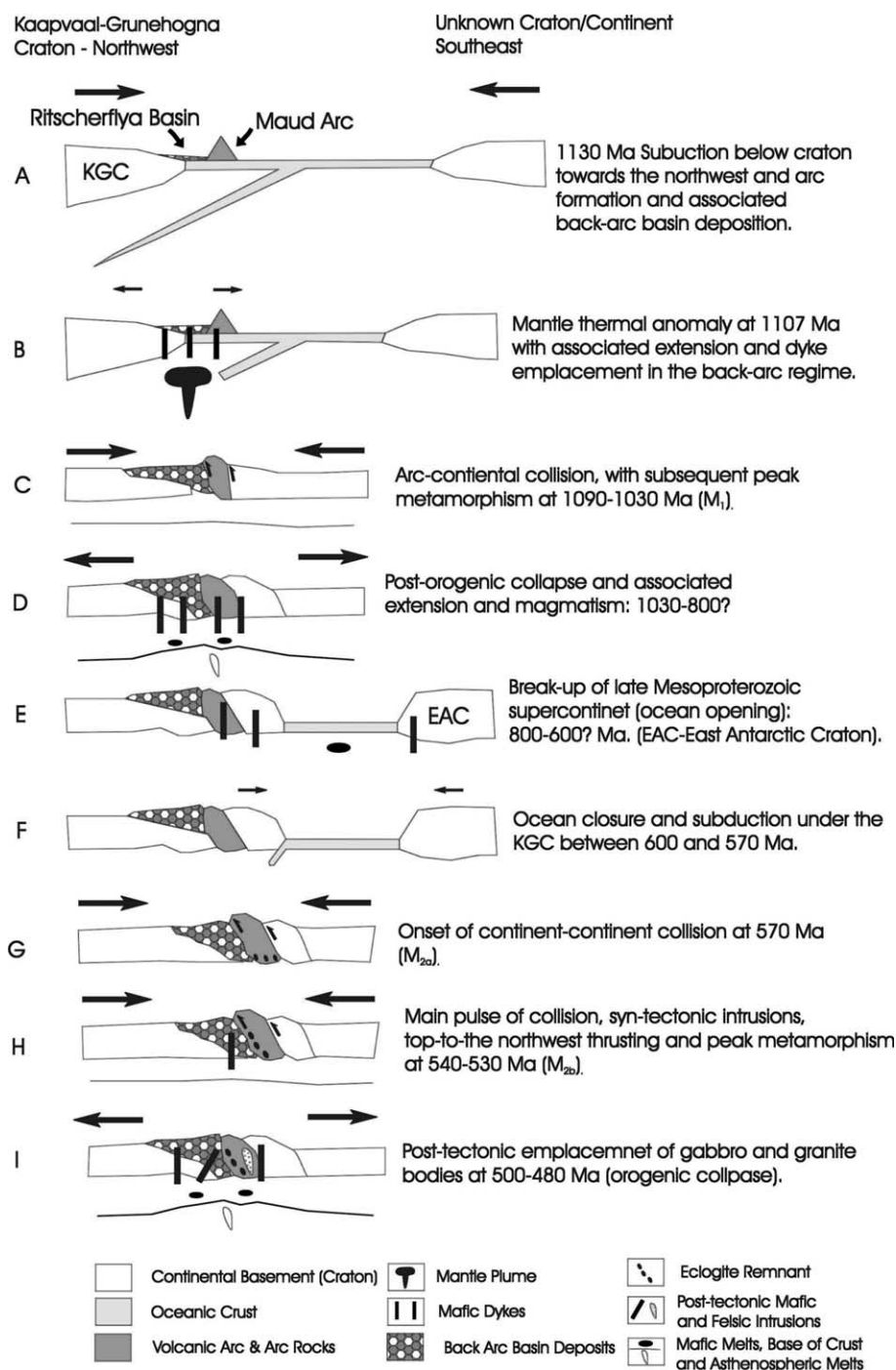


Fig. 10. Schematic diagram of the crustal evolution of western Dronning Maud Land from a Gjelsvikfjella perspective.

821 scale with examples from the Namaqua Belt (1109 ± 7 Ma; 822 Raith et al., 2003) and from a granophyre in Coats Land 823 (1106 ± 3 Ma; Gose et al., 1997). These are identical to a 824 precise age of 1105 ± 2 Ma (Hanson et al., 1998, 2004) 825 for tholeiitic sills in eastern Zimbabwe (Umkondo Prov- 826 ince) and also to that of 1102 ± 8 Ma obtained for volumi- 827 nous tholeiite emplacement in the Mid Continental Rift in 828 the southwest Grenville Orogen (Paces and Miller, 1993). 829 For the contemporaneity of these magmatic events over a 830 very large area, their cause has been ascribed to a large-

scale, but short-lived mantle thermal anomaly as previ- 831 ously proposed to explain the Umkondo magmatism 832 (Fig. 10B; Hanson et al., 1998). If decompression melting 833 of the lower crust and upper mantle were decoupled from 834 crustal plate movements, it could explain the occurrence 835 of similar and coeval magmatism in different types of con- 836 tinental crust over a large area (Frimmel, 2004). Bimodal 837 magmatism is expected for such decompression melting 838 in a presumably thinning crust. Mafic dykes, now present 839 as pre-tectonic amphibolite bodies, might well be expres- 840

sions of the same thermal event, but are awaiting precise dating.

Arc-continental collision followed, with peak metamorphic (M_1) conditions being reached at 1090 to 1030 Ma (Jacobs et al., 1998; Bisnath et al., 2004; Board et al., in press). An ophiolite complex of presumably post-Grenvillian age preserved in the northern Shackleton Range (e.g. Talarico et al., 1999) points to ocean opening between the Kalahari Craton and the East Antarctic Craton (Tessensohn et al., 1999) sometime between 1030 and 600 Ma. Bauer et al. (2003) reported 600 Ma mafic dykes in the southwestern area of the Maud Belt. New geochemical data point to similar mafic dykes being present also in the Gjelsvikfjella area (Grosch et al., 2004). The E-type MORB geochemical character (E. Grosch and A. Bisnath, unpublished data) of this magmatic event suggests oceanic basalt and mafic dyke protoliths for these pre-tectonic mafic rocks that formed in a Neoproterozoic ocean basin, possibly the Mozambique Ocean.

Closure of that ocean due to subduction (e.g. Tessensohn et al., 1999) would have led to continent–continent collision at ca. 570 Ma (M_{2a}) with the main pulse of collisional deformation, syn-tectonic magmatism and peak metamorphism (M_{2b}) between 540 and 530 Ma, involving both western and eastern Gondwana fragments. The clockwise P – T path established in this study for this period is comparable with that obtained for eclogite-bearing high-grade gneisses in the central Mozambique Belt (Sommer et al., 2003), which have been interpreted as resulting from the collision of East- and West-Gondwana. Our results support the contention of the Maud Belt representing the continuation of the East Antarctic Orogen (including the Mozambique Belt) into East Antarctica (Jacobs et al., 1998).

Preliminary Rb- and Sr-isotope data (E. Grosch and A. Bisnath, unpublished data, 2004) indicate an emplacement age of approximately 530 Ma for mafic dykes from Gjelsvikfjella, characterizing these amphibolites as syn-tectonic with respect to the final pulse of Pan-African metamorphism. This was followed by post-tectonic granite and gabbro emplacement between 500 and 480 Ma in consequence of renewed crustal thinning during a stage of post-orogenic collapse. The emplacement of dolerite dykes associated with Gondwana break-up represents the final stage in the crustal evolution of Gjelsvikfjella.

11. Uncited references

Bohlen et al. (1991), Holloway and Burnham (1972) and Sen and Bhattacharya (1984).

Acknowledgments

G. Doyle and C. Jackson are thanked for their field support and companionship during the Antarctic field seasons. E. Grosch is thanked for his assistance in the field. A.A.

Mitchell and A. Späth assisted with electron microprobe analyses at the University of Kwa-Zulu Natal, Westville Campus and at the University of Cape Town, respectively. This project was funded by a grant through the South African National Antarctic Programme (Department of Environmental Affairs & Tourism) to H.E. Frimmel. Additional funds were obtained from The Trans-Antarctica Association (TAA) to A. Bisnath.

References

- Andersen, T.B., Jamtveit, B., Dewey, J.F., Swenson, E., 1991. Subduction and exhumation of continental crust: major mechanisms during continental–continental collision and orogenic extensional collapse, a model based on the south Norwegian Caledonides. *Terra Research* 3, 303–310.
- Arima, M., Tani, K., Kawate, S., Johnston, S.T., 2001. Geochemical characteristics and tectonic setting of metamorphosed rocks in the Tugela terrane, Natal belt, South Africa. *Memoirs of National Institute of Polar Research*. V 55, 1–39.
- Arndt, N.T., Todt, W., Chauvel, C., Tapfer, M., Weber, K., 1991. U–Pb zircon age and Nd isotopic composition of granitoids, charnockites and supracrustal rocks from Heimfrontfjella, Antarctica. *Geologische Rundschau* 80, 759–777.
- Basson, I.J., Perritt, S., Watkeys, M.K., Menzies, A.H., 2004. Geochemical correlation between metasediments of the Mfongosi Group of the Natal sector of the Namaqua–Natal Metamorphic Province, South Africa and Ahlmannryggen Group of the Grunehogna Province, Antarctica. *Gondwana Research* 7, 57–73.
- Bauer, W., Jacobs, J., 2001. The Neoproterozoic Suture between East and West Gondwana—New results from central Dronning Maud Land, Antarctica. *Gondwana Research* 4, 147–149.
- Bauer, W., Jacobs, J., Fanning, C.M., Schmidt, R., 2003. Late Mesoproterozoic arc and back-arc volcanism in the Heimfrontfjella (East Antarctica) and implications for the palaeogeography at the south-eastern margin of the Kaapvaal–Grunehogna Craton. *Gondwana Research* 6, 449–465.
- Bisnath, A., Frimmel, H.E., Armstrong, R.A., 2004. Age and tectono-thermal evolution of Gjelsvikfjella, Maud Belt, East Antarctica. *Geoscience Africa 2004, Abstract Volume*, University of Witwatersrand, Johannesburg, South Africa, pp. 60–61.
- Board, W.S., Frimmel, H.E., Armstrong, R.A., in press. Pan-African tectonism in the western Maud Belt: P – T path for high-grade gneisses in the H.U. Sverdrupfjella, East Antarctica. *Journal of Petrology*.
- Bohlen, S.R., Montana, A., Kerrick, D.M., 1991. Precise determination of the equilibria kyanite=sillimanite and kyanite=andaluise and a revised triple point for Al_2SiO_5 polymorphs. *American Mineralogist* 76, 677–680.
- Bucher, K., Frey, M., 1994. *Petrogenesis of Metamorphic Rocks*, sixth ed. Springer-Verlag, Berlin, p. 318.
- Bucher-Nurminen, K., Ohta, Y., 1993. Granulites and garnet-cordierite gneisses from Dronning Maud Land, Antarctica. *Journal of Metamorphic Geology* 11, 691–703.
- Cornell, D.H., Thomas, R.J., Bowring, S.A., Armstrong, R.A., Gramham, G.H., 1996. Protolith interpretation in metamorphic terranes: a back-arc environment with Besshi-type base metal potential for the Quha formation, Natal Province, South Africa. *Precambrian Research* 77, 243–271.
- Dalziel, I.W.D., 1997. Neoproterozoic–Palaeozoic geography and tectonics: review, hypothesis and environmental speculation. *Geological Society of America. Bulletin* 109, 16–42.
- Engvik, A.K., Elvevold, S., 2004. Pan-African extension and near-isothermal exhumation of a granulite facies terrain, Dronning Maud Land, Antarctica. *Geological Magazine* 141, 649–660.

- 956 Ferrar, G.R., 1995. The metamorphic geology of the Årsmålsryggen,
957 northern Kirwanveggen, western Dronning Maud Land, Antarctica.
958 Unpublished M.Sc. Thesis, University of Natal, Pietermaritzburg.
- 959 Frimmel, H. E., 2004. Formation of a late Mesoproterozoic superconti-
960 nent: the South Africa–East Antarctica connection. In: Eriksson, P.G.,
961 Altermann, W., Nelson, D.R., Mueller, W.U., Catuneanu, O. (Eds.),
962 The Precambrian Earth: Tempos and Events. Developments in
963 Precambrian Geology, vol. 12, Elsevier, Amsterdam, pp. 240–255.
- 964 Gose, W.A., Dalziel, I.W.D., Helper, M.A., Hutson, F., Connelly, J.,
965 1997. Paleomagnetic data and U–Pb isotopic age determinations from
966 Coats Land, Antarctica: implications for late Proterozoic reconstruc-
967 tions. *Journal of Geophysical Research* 102 (B4), 7887–7902.
- 968 Graham, C.M., Powell, R., 1984. A garnet-hornblende geothermometer:
969 calibration, testing, and application to the Pelona Schist, South
970 California. *Journal of Metamorphic Geology* 2, 13–31.
- 971 Grantham, G.H., Jackson, C., Moyes, A.B., Groenewald, P.B., Harris,
972 P.D., Ferrar, G., Krynauw, J.R., 1995. The tectonothermal evolution
973 of the Kirwanveggen–H.U. Sverdrupfjella area, Dronning Maud
974 Land, Antarctica. *Precambrian Research* 75, 209–229.
- 975 Groenewald, P.B., Hunter, D.R., 1991. Granulites of the northern H.U.
976 Sverdrupfjella, western Dronning Maud Land: metamorphic history
977 from garnet-pyroxene assemblages, coronas and hydration reactions.
978 In: Thompson, M.R.A., Crame, J.A., Thomson, J.W. (Eds.), *Geologi-
979 cal evolution of Antarctica*. Cambridge University Press, Cambridge,
980 pp. 61–66.
- 981 Groenewald, P.B., Moyes, A.B., Grantham, G.H., Krynauw, J.R., 1995.
982 East Antarctic crustal evolution: geological constraints and modelling
983 in western Dronning Maud Land. *Precambrian Research* 75, 231–250.
- 984 Grosch, E.G., Bisnath, A., Frimmel, H.E., Board, W.S., 2004. Geochem-
985 istry and tectonic setting of Proterozoic mafic rocks in western
986 Dronning Maud Land, Antarctica. *Geoscience Africa 2004*, Abstract
987 Volume, University of Witwatersrand, Johannesburg, South Africa,
988 pp. 229–230.
- 989 Hanson, R.E., Martin, M.W., Bowring, S.A., Munyanyiwa, H., 1998. U–
990 Pb zircon age for the Umkondo dolerites, eastern Zimbabwe: 1.1 Ga
991 large igneous province in Southern Africa–East Antarctica and
992 possible Rodinia correlations. *Geology* 26, 1143–1146.
- 993 Hanson, R.E., Crowley, J.L., Bowring, S.A., Ramezani, J., Cose, W.A.,
994 Dalziel, I.W.D., Pancake, J.A., Seidel, E.K., Blenkinsop, Thomas, G.,
995 Mukwakwami, J., 2004. Coeval large-scale magmatism in the Kalahari
996 and Laurentian cratons during Rodinia assembly. *Science* 304, 1126–
997 1129.
- 998 Harris, P.D., 1999. The geological evolution of Neumayerskarvet in the
999 Northern Kirwanveggen, Western Dronning Maud Land, Antarctica.
1000 Unpublished Ph.D. Thesis, Rand Afrikaans University, Johannesburg.
- 1001 Harris, P.D., Moyes, A.B., Fanning, C.M., Armstrong, R.A., 1995. Zircon
1002 ion microprobe results from the Maudheim high-grade gneiss terrane,
1003 western Dronning Maud Land, Antarctica: Centennial Geocongress
1004 (1995), Johannesburg, pp. 240–243.
- 1005 Hoffman, P.F., 1991. Did the breakout of Laurentia turn Gondwana
1006 inside-out? *Science* 252, 1409–1412.
- 1007 Holland, T., Blundy, J., 1994. Non-ideal interactions in calcic amphiboles
1008 and their bearing on amphibole-plagioclase thermometry. *Contribu-
1009 tions to Mineralogy and Petrology* 116, 433–447.
- 1010 Holloway, J.R., Burnham, C.W., 1972. Melting relationship of basalt with
1011 equilibrium water pressure less than total pressure. *Journal of
1012 Petrology* 13, 1–29.
- 1013 Jackson, C., 1999. Characterization of Mesoproterozoic to Palaeozoic
1014 crustal evolution of western Dronning Maud Land. Study 3: Deforma-
1015 tional history and thermochronology of the central Kirwanveggen.
1016 Unpublished Report, Department of Environmental Affairs and
1017 Tourism, Pretoria, p. 80.
- 1018 Jacobs, J., Thomas, R.J., 1994. Oblique collision at about 1.1 Ga along the
1019 southern margin of the Kaapvaal continent, south-east Africa.
1020 *Geologische Rundschau* 83, 322–333.
- 1021 Jacobs, J., Thomas, R.J., Weber, K., 1993. Accretion and indentation
1022 tectonics at the southern edge of the Kaapvaal craton during the
1023 Kibaran (Grenville orogen). *Geology* 21, 203–206.
- Jacobs, J., Bauer, W., Spaeth, G., Thomas, R.J., Weber, K., 1996. 1024
Lithology and structure of the Grenville-aged (1.1 Ga) basement of 1025
Heimefrontjella (East Antarctica). *Geologische Rundschau* 85, 800– 1026
821.
- Jacobs, J., Fanning, C.M., Henjes-Kunst, F., Olesch, M., Paech, H.-J., 1027
1998. Continuation of the Mozambique Belt into East Antarctica: 1028
Grenville-age metamorphism and polyphase Pan-African high-grade 1029
events in central Dronning Maud Land. *Journal of Geology* 106, 385– 1030
406.
- Jacobs, J., Hansen, B.T., Henjes-Kunst, F., Thomas, R.J., Bauer, W., 1031
Weber, K., Armstrong, R.A., Cornell, D.H., 1999. New age con- 1032
straints on Proterozoic/lower Palaeozoic evolution of Heimfrontfjella, 1033
East Antarctica, and its bearing on Rodinia/Gondwana correlations. 1034
Terra Antarctica 6, 377–389.
- Jacobs, J., Fanning, C.M., Bauer, W., 2003a. Timing of Grenville-age vs 1035
Pan-African medium- to high-grade metamorphism in western Dron- 1036
ning Maud Land (East Antarctica) and significance for correlations in 1037
Rodinia and Gondwana. *Precambrian Research* 125, 1–20. 1038
- Jacobs, J., Bauer, W., Fanning, C.M., 2003b. Late Neoproterozoic/Early 1039
Palaeozoic events in central Dronning Maud Land and significance for 1040
the southern extension of the East African Orogen into East 1041
Antarctica. *Precambrian Research* 126, 27–53. 1042
- Jacobs, J., Klemd, R., Fanning, C. M., Bauer, W., Colombo, F., 2003c. 1043
Extensional collapse of the late Neoproterozoic–early Palaeozoic East 1044
African–Antarctic Orogen in central Dronning Maud Land, East 1045
Antarctica. In: Yoshida, M., Windley, B.F., Dasgupta, S. (Eds.) 1046
Proterozoic East Gondwana: Supercontinent Assembly and Breakup, 1047
Geological Society, London. Special Publication 206, pp. 271–285. 1048
- Jacobs, J., Bauer, W., Fanning, C.M., 2003d. New age constraints for 1049
Grenvillian age metamorphism in western central Dronning Maud 1050
Land (East Antarctica), and implications for the palaeogeography of 1051
Kalahari in Rodinia. *International Journal of Earth. Science* 92, 301– 1052
315. 1053
- Johnston, S.T., Armstrong, R., Heaman, L., McCourt, S., Mitchell, A., 1054
Bisnath, A., Arima, M., 2001. Preliminary U–Pb geochronology of the 1055
Tugela terrane, Natal belt, eastern South Africa. *Memoirs of National 1056
Institute of Polar Research* 55, 40–58. 1057
- Kohn, M.J., Spear, F.S., 1990. Two new geobarometers for garnet 1058
amphibolites, with application to southeastern Vermont. *American 1059
Mineralogist* 75, 89–96. 1060
- Kohn, M.J., Spear, F.S., 2000. Retrograde net transfer reaction insurance 1061
for pressure–temperature estimates. *Geology* 28, 1127–1130. 1062
- Kretz, R., 1983. Symbols for rock forming minerals. *American Mineral- 1063
ogist* 68, 277–279. 1064
- Krynauw, J.R., 1996. A review of the geology of east Antarctica, with 1065
special reference to the c. 1000 Ma and c. 500 Ma events. *Terra 1066
Antarctica* 3, 77–89. 1067
- Leake, B.E., Woolley, A.R., Arps, C.E.S., Birch, W.D., Gilbert, M.C., 1068
Grice, J.D., Hawthorne, F.C., Kato, A., Kisch, H.J., Krivovichev, 1069
V.G., Linthout, K., Laird, J., Mandarion, J., Maresch, W.V., Nickel, 1070
E.H., Rock, N.M.S., Schumacher, J.C., Smith, D.C., Stephenson, 1071
N.C.N., Ungaretti, L., Whittaker, E.J.W., Youzhi, G., 1987. Nomen- 1072
clature of Amphiboles: report of the Subcommittee on Amphiboles of 1073
the International Mineralogical Association Commission on New 1074
Minerals and Mineral Names. *Mineralogical Magazine* 61, 295–321. 1075
- Meert, J.G., 2003. A synopsis of events related to the assembly of Eastern 1076
Gondwana. *Tectonophysics* 362, 1–40. 1077
- Meert, J.G., Van der Voo, R., 1997. The assembly of Gondwana 800– 1078
550 Ma. *Journal of Geodynamics* 23, 223–235. 1079
- Messiga, B., Tribuzio, R., Vannucci, R., 1990. Mafic and ultramafic pods 1080
with eclogitic relics from the Proterozoic Nagsugtoqidian mobile belt 1081
of East Greenland. *Lithos* 25, 101–118. 1082
- Morimoto, N., 1998. Nomenclature of pyroxenes. *Schweizerische Miner- 1083
alogische und Petrographische Mitteilungen* 68, 95–111. 1084
- Moyes, A.B., Groenewald, P.B., 1996. Isotopic constraints on Pan- 1085
African metamorphism in Dronning Maud Land, Antarctica. *Chem- 1086
ical Geology* 129, 247–256. 1087
1088
1089
1090

- 1091 Ohta, Y. (Ed.), 1999. Nature Environment Map, Dronning Maud Land, 1129
 1092 Gjelsvikfjella & western Mühlig-Hofmannfjella 1:100000. Norsk 1130
 1093 Polarinst. TEMAKART, Nr. 24, 1999. 1131
 1094 Ohta, Y., Tørudbakken, B.O., Shiraishi, K., 1990. Geology of Gjelsvikfj- 1132
 1095 ella and Western Mühlig-Hofmannfjella, Dronning Maud Land, east 1133
 1096 Antarctica. Polar Research 8, 99–126. 1134
 1097 Owada, M., Baba, S., Läufer, L., Elvevold, S., Shiraishi, K., Jacobs, J., 1135
 1098 2003. Geology of eastern Mühlig-Hofmannfjella and Filchnerfjella in 1136
 1099 Dronning Maud Land, East Antarctica: a preliminary report on the 1137
 1100 Japan–Norway–Germany joint geological investigation. Polar Geosci- 1138
 1101 ence 16, 108–136. 1139
 1102 Paces, J.B., Miller, J.D., 1993. Precise U–Pb ages of Duluth Complex and 1140
 1103 related mafic intrusions, Northeastern Minnesota: Geochronological 1141
 1104 insights to physical, petrogenic, and paleomagnetic and tectonomag- 1142
 1105 netic processes associated with the 1.1 Ga mid-continent rift system. 1143
 1106 Journal of Geophysical Research 98B, 13997–14013. 1144
 1107 Pattison, D.R.M., Chacko, T., Farquhar, J., McFarlane, C.R.M., 2003. 1145
 1108 Temperatures of granulite-facies metamorphism: constraints from 1146
 1109 experimental phase equilibria and thermobarometry corrected for 1147
 1110 retrograde exchange. Journal of Petrology 44, 867–900. 1148
 1111 Paulsson, O., Austrheim, H., 2003. A geochronological and geochemical 1149
 1112 study of rocks from Gjelsvikfjella, Dronning Maud Land, Antarctica- 1150
 1113 implications for Mesoproterozoic correlations and assembly of Gondw- 1151
 1114 ana. Precambrian Research 125, 113–138. 1152
 1115 Powell, R., Holland, T., 1994. Optimal geothermometry and geobarom- 1153
 1116 etry. American Mineralogist 79, 120–133. 1154
 1117 Powell, R., Holland, T., Worley, B., 1998. Calculating phase diagrams 1155
 1118 involving solid solutions via non-linear equations, with examples using 1156
 1119 THERMOCALC. Journal of Metamorphic Petrology 16, 577–588. 1157
 1120 Raith, J.G., Cornell, D.H., Frimmel, H.E., de Beer, C.H., 2003. New 1158
 1121 insights into the geology of the Namaqua Tectonic Province, South 1159
 1122 Africa, from ion probe dating of detrital and metamorphic zircon. 1160
 1123 Journal of Geology 111, 347–366. 1161
 1124 Ramsay, J.G., 1967. Folding and Fracturing of Rocks. McGraw-Hill, 1162
 1125 New York, 567 pp. 1163
 1126 Sen, S.K., Bhattacharya, A., 1984. An orthopyroxene-garnet thermometer 1164
 1127 and its application to the Madras charnockites. Contributions to
 1128 Mineralogy and Petrology 88, 64–71.
- Sommer, H., Kröner, A., Hauzenberger, C., Muhongo, S., Wingate, 1129
 M.T.D., 2003. Metamorphic petrology and zircon geochronology of 1130
 high-grade rocks from the central Mozambique Belt of Tanzania: 1131
 crustal recycling of Archean and Palaeoproterozoic material during the 1132
 Pan-African orogeny. Journal of metamorphic Geology 21, 915–934. 1133
 Spear, F.S., 1993. Metamorphic phase equilibria and pressure–tempera- 1134
 ture–time paths. Mineralogical Society of America, Monograph 799. 1135
 Spear, F.S., Florence, F.P., 1992. Thermobarometry in granulites: pitfalls 1136
 and new approaches. In: van Reenan, D.D., Roering, C., Ashwal, 1137
 L.D., de Wit, M.J. (Eds.), The Archean Limpopo Granulite Belt: 1138
 Tectonics and Deep Crustal Processes. Precambrian Research 55, 209– 1139
 241. 1140
 Talarico, F., Kleinschmidt, G., Henjes-Kunst, F., 1999. An ophiolite 1141
 complex in the northern Shackleton range, Antarctica. Terra Antarc- 1142
 tica 6, 317–325. 1143
 Tessensohn, F., Kleinschmidt, G., Talarico, F., Buggisch, W., Brommer, 1144
 A., Henjes-Kunst, F., Kroner, U., Millar, I.L., Zeh, A., 1999. Ross-age 1145
 amalgamation of East and West Gondwana: evidence from the 1146
 Shackleton Range, Antarctica. Terra Antarctica 6, 317–325. 1147
 Thomas, R.J., Cornell, D.H., Armstrong, R.A., 1999. Provenance age and 1148
 metamorphic history of the Quha Formation, Natal Metamorphic 1149
 Province: a U–Th–Pb zircon SHRIMP study. South African Journal 1150
 of Geology 102, 83–88. 1151
 Tingey, R.J., 1991. The regional geology of Archaean and Proterozoic 1152
 rocks in Antarctica. In: Tingey, R.J. (Ed.), The Geology of Antarctica. 1153
 Oxford University Press, Oxford, pp. 1–73. 1154
 White, R.W., Powell, R., Holland, T.J.B., 2001. Calculations of partial 1155
 melting equilibria in the system Na₂O–CaO–K₂O–FeO–MgO–Al₂O₃– 1156
 SiO₂–H₂O (NCKFMASH). Journal of Metamorphic Petrology 19, 1157
 139–153. 1158
 Wolmarans, L.G., Kent, L.E., 1982. Geological investigations in Western 1159
 Dronning Maud Land, Antarctica—a synthesis. South African Jour- 1160
 nal of Antarctic Research (Supplement 2), 93. 1161
 Yardley, B.W.D., 1991. An Introduction to Metamorphic Petrology. John 1162
 Wiley and Sons, New York, p. 248. 1163
 1164